Global and Planetary Change 235 (2024) 104393

Contents lists available at ScienceDirect

Global and Planetary Change

journal homepage: www.elsevier.com/locate/gloplacha

Evaluating the isotopic composition of leaf organic compounds in fog-dependent *Tillandsia landbeckii* across the coastal Atacama Desert: Implications for hydroclimate reconstructions at the dry limit

Andrea Jaeschke [a,*], Christoph Böhm [b], Jan H. Schween [b], Enno Schefuß [c], Marcus A. Koch [d,e], Claudio Latorre [f,g], Sergio Contreras [h,i], Janet Rethemeyer [a], Holger Wissel [j], Andreas Lücke [j]

[a] *Institute of Geology and Mineralogy, University of Cologne, Germany*
[b] *Institute for Geophysics and Meteorology, University of Cologne, Germany*
[c] *MARUM - Center for Marine Environmental Sciences, University of Bremen, Germany*
[d] *Centre for Organismal Studies (COS), Heidelberg University, 69120 Heidelberg, Germany*
[e] *Heidelberg Center for the Environment (HCE), Heidelberg University, 69120 Heidelberg, Germany*
[f] *Centro UC Desierto de Atacama & Facultad de Ciencias Biológicas, Pontificia Universidad Católica de Chile, Chile*
[g] *Institute of Ecology & Biodiversity (IEB), Santiago, Chile*
[h] *Departamento de Química Ambiental, Facultad de Ciencias, Universidad Católica de la Santísima Concepción, Concepción, Chile*
[i] *Centro de Investigación en Biodiversidad y Ambientes Sustentables, CIBAS, Concepción, Chile*
[j] *Institute of Bio- and Geosciences, Agrosphere Institute (IBG-3), Forschungszentrum Jülich GmbH, Germany*

ARTICLE INFO

Editor: Liviu Matenco

Keywords:
Atacama Desert
Fog
Tillandsia landbeckii
CAM
N-alkanes
Cellulose
Stable isotopes

ABSTRACT

Fog is an important component of the coastal climate of northern Chile and southern Peru. Moisture and nutrients from fog maintain highly endemic vegetation (lomas) as well as unique *Tillandsia landbeckii* ecosystems that thrive at elevations of ca. 900–1200 m asl. Although this epiphytic CAM bromeliad is well adapted to the extreme climate, declining *Tillandsia* stocks observed over the past decades question the long-term survival with ongoing climate change. Here, we aim at better understanding the hydroclimatic signal encoded in the leaf organic compounds of *Tillandsia landbeckii* across the Atacama Desert's coastal mountain range (ca. 18–21°S). First, we investigate spatiotemporal patterns of fog occurrence and related moisture sources available for the plants applying a new satellite-based fog-detection approach. We then use stable carbon, oxygen and hydrogen ($\delta^{13}C$, $\delta^{18}O$, δD) isotope analysis of leaf wax *n*-alkanes and cellulose to identify photosynthetic pathway as well as environmental and physiological processes that shape the isotopic composition in *Tillandsia landbeckii*. We find that leaf wax *n*-alkanes and cellulose reflect the balance of climatic and physiological drivers differently. While *n*-alkane δD values more closely follow changes in precipitation δD, evaporative enrichment seems to have a dominant influence on cellulose $\delta^{18}O$ values. Cellulose δD values are highly enriched compared to *n*-alkane δD values, likely reflecting a predominant metabolic imprint on δD. $\delta^{13}C$ signatures in the organic compounds are valid proxies for CAM activity. Our results prove the general applicability of the isotopic biomarkers for reconstructing environmental change in the coastal Atacama Desert. This approach can be extended globally to west-coast deserts that share fog as a major source of moisture.

1. Introduction

Fog is an important component in the water budget of many coastal regions and montane forests worldwide and provides the ultimate moisture and nutrient source for unique ecosystems in the coastal deserts of northern Chile and Namibia (Aravena et al., 1989; Pinto et al., 2006; Soderberg, 2010; Scholl et al., 2011; Evans et al., 2019; Del Rio et al., 2021). In the hyperarid Atacama Desert, where annual precipitation rates are <2 mm/yr (Houston, 2006), even low amounts of fog water may have an effect on ecosystem functioning and productivity in an otherwise barren landscape (Rundel et al., 1997; Pinto et al., 2006; García et al., 2021). Here, fog is frequently formed when the marine

* Corresponding author.
E-mail address: andrea.jaeschke@uni-koeln.de (A. Jaeschke).

https://doi.org/10.1016/j.gloplacha.2024.104393
Received 1 May 2023; Received in revised form 13 February 2024; Accepted 24 February 2024
Available online 28 February 2024

stratocumulus cloud deck intercepts with the steep topography of the coastal mountain range (Cereceda et al., 2008; Del Rio et al., 2018; Schween et al., 2020; Böhm et al., 2021). Natural oases form in the fog zone and support rich, highly endemic lomas vegetation (Rundel et al., 1997; Rundel and Dillon, 1998). *Tillandsia landbeckii* (hereafter *T. landbeckii*), an epiphytic bromeliad, is often found between 900 and 1200 m above sea level (asl) and is well adapted to the harsh environmental conditions typical of the coastal Atacama Desert. These plants form almost mono-specific self-organized dune ecosystems known locally as 'tillandsiales' by trapping sand and "raising" themselves up on the surface of coppice dunes to maximize their interception with fog moisture (Borthagaray et al., 2010). With a distribution highly sensitive to spatiotemporal variations in fog occurrence, the plants act as "biosensors" of fog water availability (Pinto et al., 2006; Latorre et al., 2011; Jaeschke et al., 2019; Koch et al., 2020; García et al., 2021). Recent observations, however, point to changes in fog occurrence above/below a certain threshold at ~1000 m asl (Del Rio et al., 2021) resulting from a decreasing height of the thermal inversion layer over the ocean, i.e., the top of the stratocumulus cloud in recent decades (Schulz et al., 2011; Muñoz et al., 2016). This change in fog occurrence with respect to frequency, duration and water content may impact the narrow elevational range in which *T. landbeckii* ecosystems are distributed. As a result, severe dehydration and dieback of 'tillandsiales' has been noticed over recent decades (Rundel et al., 1997; Pinto et al., 2006; Schulz et al., 2011).

Desert plants are subject to a wide range of abiotic stresses, such as extreme water limitation, evaporation and high solar radiation. The metabolism and physiology of CAM (crassulacean acid metabolism) plants is adapted to high stress tolerance and thus crucial for survival at the extreme dry limit (Dodd et al., 2002; Haslam et al., 2003; Lüttge, 2004; Hermida-Carrera et al., 2020). *T. landbeckii* lack functional roots (epiarenic) and use sand as stabilizing substrate of the shoot/leaf system (Rundel et al., 1997; Rundel and Dillon, 1998; Koch et al., 2019, 2020). The plants absorb liquid water directly via foliar trichomes, which cover the whole leaf surface (Benzing et al., 1978; Schmitt et al., 1989; Raux et al., 2020). The greatest benefit of CAM is believed to be increased water use efficiency (Lange and Medina, 1979; Cushman, 2001; Lüttge, 2010). The CAM pathway is characterized by the temporal separation of carbon fixation modes compared to the spatial separation in C_4 plants (e.g., Cushman, 2001). Stomatal opening is restricted to the night minimizing water loss during CO_2 acquisition. Water harvesting is most effective during the night, when most fog events occur. On the other hand, too much moisture may also affect efficient gas exchange and thus hinder plant growth (Benzing et al., 1978; Martin, 1994). CO_2 assimilation then follows during the light period when stomata are closed, thereby minimizing water loss during the day. As a consequence of stomatal limitations and thus very low intercellular CO_2 levels, photosynthetic rates, growth and biomass productivity of CAM plants are low compared to C_3 or C_4 plants (Ehleringer et al., 1998; Lüttge, 2004; Koch et al., 2020). Although CAM plants are relatively rare globally (ca. 7% of all vascular plants; Hermida-Carrera et al., 2020), they are able to inhabit diverse niches in the tropics (Lüttge, 2010) and represent the most dominant fraction of vegetation in isolated regions of the coastal Atacama Desert (Rundel et al., 1997; Pinto et al., 2006). *T. landbeckii* is a long-lived perennial plant, therefore, the molecular and isotopic information encoded in leaves and organic compounds of modern plants may record decadal to centennial changes in hydroclimate. Buried plant remains may carry climate information for the past 3500 years or even longer (Latorre et al., 2011; Jaeschke et al., 2019; Contreras et al., 2022).

Water and plant growth are intrinsically linked to each other. The stable isotopes of carbon ($\delta^{13}C$) and water ($\delta^{2}H$ or δD, and $\delta^{18}O$) analyzed in the organic matter of plants such as whole leaves, leaf waxes or cellulose, can provide insights in carbon sources, photosynthetic carbon fixation type (e.g., C_3 vs C_4) and hydrology (e.g., water sources) and thus are useful tools to evaluate the ecosystem response to present and past climate changes (Epstein et al., 1977; Schefuß et al., 2005; Diefendorf and Freimuth, 2017; Kock et al., 2019; Arosio et al., 2020). Long-chain *n*-alkanes are major lipid components of the cuticular wax layer of terrestrial higher plants (Eglinton and Hamilton, 1967). They provide a protective barrier against water loss through the cuticle and UV-radiation damage, and regulate gas exchange (Jetter et al., 2006; Koch and Ensikat, 2008). In *T. landbeckii*, about 97% of the total leaf surface is covered by an impermeable leaf wax layer while trichomes represent only 3% (Raux et al., 2020). The hydrogen isotope composition of plant leaf waxes (δD_{wax}) has been proposed to record the isotope composition of the plant's source water (δD_p), affected by secondary factors, such as vegetation type, evapotranspiration and environmental conditions (e.g., Sachse et al., 2012). Only few studies investigated δD_{wax} in CAM plants (Sternberg et al., 1984; Chikaraishi and Naraoka, 2003; Feakins and Sessions, 2010a, 2010b), likely because CAM plants are relatively rare compared to C_3 or C_4 plants and the metabolism shares features with both C_3 and C_4 plants thus complicating a straight forward interpretation of the isotopic signal stored in the molecules. In addition, many C_3/CAM intermediate plants can switch between photosynthetic modes and use variable degrees of CAM depending on environmental dynamics (Feakins and Sessions, 2010b; Lüttge, 2010; Hermida-Carrera et al., 2020). The few existing studies that analyzed either long-chain *n*-alkanes or total extractable lipids in CAM plants, however, found that δD values are comparable to those of C_3 plants (Sternberg et al., 1984; Hayes, 2001; Feakins and Sessions, 2010b). In contrast, δD values of cellulose nitrate are typically higher in CAM plants compared to C_3 plants, suggesting that CAM has a significant impact on biochemical D-fractionation during carbohydrate metabolism prior to cellulose synthesis (Sternberg et al., 1984; Hayes, 2001; Feakins and Sessions, 2010b; Cormier et al., 2018, 2019).

To our knowledge, comprehensive studies evaluating water isotope ratios in leaf waxes or cellulose of CAM plants from the hyperarid Atacama Desert are missing. In a previous study, Contreras et al. (2022) investigated the composition and distribution of leaf wax *n*-alkanes and fatty acids in *T. landbeckii*, which already indicated fine-scale molecular adaptations along a precipitation gradient in the coastal Atacama Desert. Here, we aim at better understanding the hydroclimatic signal encoded in the leaf organic compounds of the plants. The objectives of this study were therefore to 1) investigate spatio-temporal patterns of fog occurrence and related moisture sources available for the different *T. landbeckii* dune ecosystems, and 2) evaluate the isotopic response of the plant organic compounds to extremely low water supply across environmental gradients. To achieve this, we generated a 19-year monthly fog climatology for each *T. landbeckii* site applying a new satellite-based fog-detection approach by Böhm et al. (2021). $\delta^{13}C$, $\delta^{18}O$ and δD measurements of both leaf wax *n*-alkanes and cellulose were used to identify photosynthetic pathway as well as environmental and physiological processes that shape the isotopic composition in *T. landbeckii*. We document significant relationships of the organic compounds' isotopic compositions with changes in fog occurrence, precipitation δD and $\delta^{18}O$ across the coastal transect, and provide first insights in the applicability of the different hydrological proxies.

2. Materials and methods

2.1. Study area and sampling strategy

The study area is located in the Coastal Cordillera of the Chilean Atacama Desert (Fig. 1). The coastal mountain range with elevations of approximately 1000–1600 m asl separates the narrow coastal plain from the broad Central Valley (Houston and Hartley, 2003). The climate regime is influenced by 1) the presence of the southeast Pacific anticyclone, maintained by large-scale air subsidence 2) the cold Humboldt current and coastal upwelling, and 3) the rain shadow effect of the Andes resulting in a very dry and stable coastal climate with almost uniform annual air temperature of 18–19 °C (Houston and Hartley,

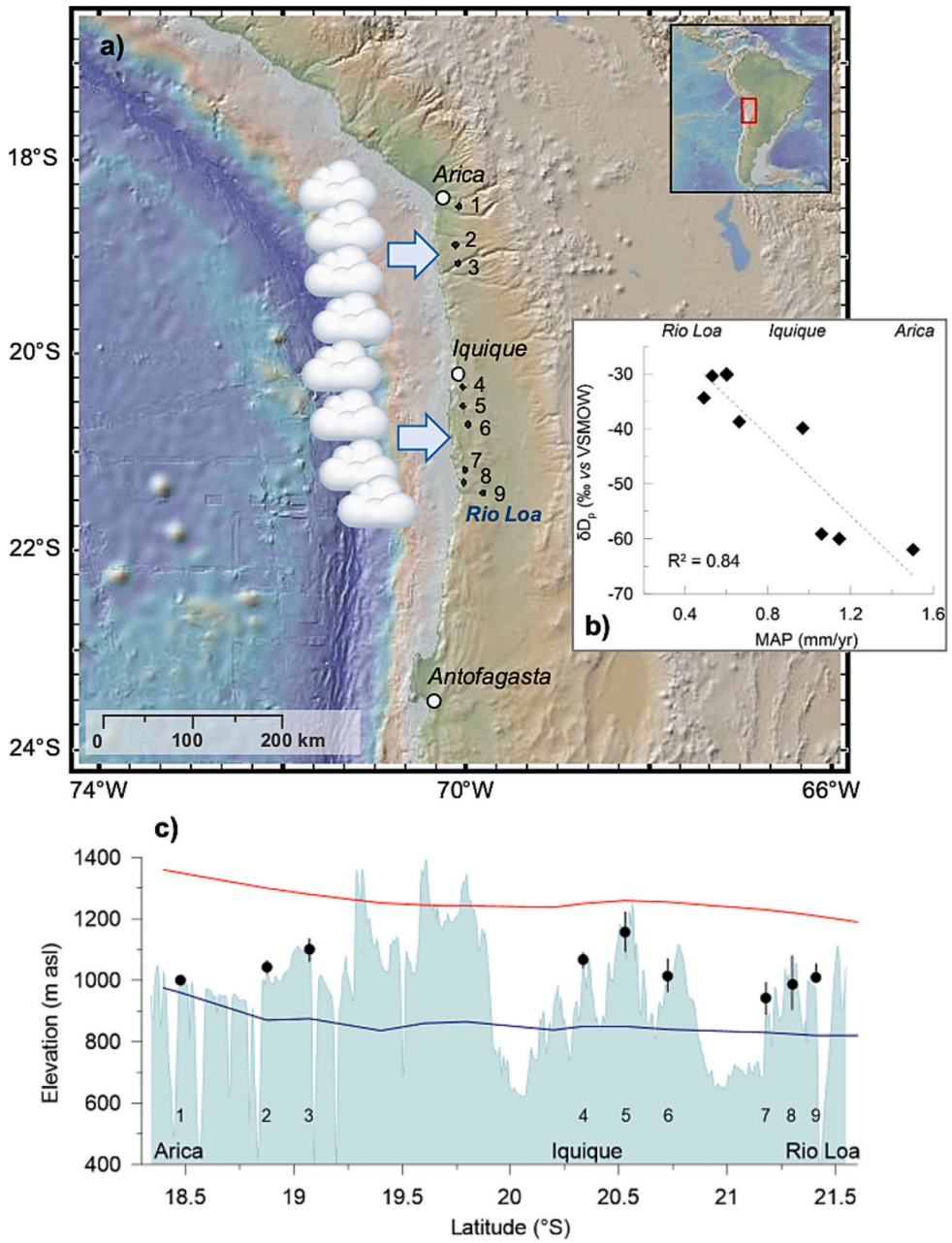

Fig. 1. a) Map of the study area with locations of the nine *T. landbeckii* sites along the coastal Atacama Desert in northern Chile. Blue arrows indicate transport of the marine stratocumulus cloud deck toward the coastal mountain range; b) Relationship between mean annual precipitation (MAP) estimates (Jaeschke et al., 2019; Reyers, 2019) and mean annual hydrogen isotopic composition of precipitation (δD_p) obtained for each site using OIPC (Bowen and Revenaugh, 2003; Bowen, 2022); c) Coastal topographic profile showing the position of *T. landbeckii* sites within the low cloud/fog zone. Cloud base/top are indicated by blue/red lines. Sites 1–3 and 9 are located at canyons (Jaeschke et al., 2019). (For interpretation of the references to colour in this figure legend, the reader is referred to the web version of this article.)

2003; Garreaud et al., 2008; Schulz et al., 2011). Annual precipitation in the study area is extremely low (Fig. 1b) but larger rainfall events occur irregularly during El Niño years also at the coast (Houston, 2006; Garreaud et al., 2008; Jordan et al., 2019; Reyers et al., 2021). At present, estimates of the isotopic composition of precipitation according to Bowen (2022) shows a negative correlation with mean annual precipitation along the investigated latitudinal gradient (Fig. 1b). This indicates that δD_p is determined by the amount effect as expected in low-latitude maritime regions (Dansgaard, 1964; Araguás-Araguás et al., 2000; Kurita et al., 2009).

Fog is frequently formed when the marine stratocumulus intercepts with the steep topography of the coastal mountain range (Garreaud et al., 2008; Lobos-Roco et al., 2018; Schween et al., 2020). Advection of marine air masses facilitate fog formation further inland at night and early morning (Schween et al., 2020), while changes in air circulation during the afternoon produces thermal stratification that dissipates fog (Muñoz et al., 2016; Lobos-Roco et al., 2018). The seasonality of the annual fog cycle is primarily determined by the large-scale air subsidence and spatial distribution of coastal sea surface temperatures (Schween et al., 2022). During austral winter, the stratocumulus cloud is thicker and contains more water but also occurs at lower elevation compared to austral summer (Cereceda et al., 2008; Del Rio et al., 2018; García et al., 2021; Schween et al., 2022). Moreover, fog may still penetrate further inland, where the coastal cliff is intercepted by

canyons (sites 1–3, 9) or is generally lower in elevation (sites 5, 6) (Fig. 2; Supplementary Fig. 1). Fog water levels may exceed those of rainfall but are less well constrained. The only estimate for fog water flux per surface area is 25 mm/yr based on a few days of turbulent flux measurements in fog above a *T. landbeckii* carpet at site 4 (Fig. 1) (Westbeld et al., 2009). Other measurements with fog collectors provide fog water yields ranging from 2l/m^2/yr (González et al., 2011) for *T. landbeckii* fields several km from the coast to ca. 2500l/m^2/yr at Alto Patache directly at the coastal cliff (Cereceda et al., 2008; García et al., 2021). But it has to be noted that these values are valid for the fog collectors oriented more or less perpendicular to the wind and not for the surface, i.e., these data cannot be directly compared with precipitation data.

We examined *T. landbeckii* population systems at nine different sites (Rundel et al., 1997; Pinto et al., 2006) irregularly distributed along the coastal mountain range at elevations of approximately 900–1200 m asl between Arica and the Rio Loa canyon and reaching approximately 3–27 km inland (ca. 18.5°S - 21.5°S; Fig. 1c). Observations from the field indicate increased dieback of the plants at lower elevations most likely abandoned from fog during recent decades (Koch et al., 2020; García et al., 2021; Jaeschke et al., 2023). *T. landbeckii* form either continuous units or sparse and isolated stands on W and SW facing slopes directly exposed to fog covering areas of 0.6–18.5 km^2 (Pinto et al., 2006; Borthagaray et al., 2010; Koch et al., 2020). The sampling approach was designed to cover a range in latitude, altitude, and distance to the coast and to account for heterogeneity (Jaeschke et al., 2019). In total 87 *T. landbeckii* specimens were collected in March 2017, air dried and shipped to Germany for further processing and analyses.

2.2. Fog detection

A new satellite-based fog retrieval approach was applied according to the method described by Böhm et al. (2021). Briefly, it utilizes an artificial neural network to exploit satellite observations, namely radiances at different wavelengths in the infrared spectrum from the Moderate Resolution Imaging Spectroradiometer (MODIS) installed on the *Terra* and *Aqua* satellites (level-1B 1-km Calibrated Radiances Product: MOD021KM, MYD021KM; MODIS Characterization Support Team, 2017a, 2017b). To infer the fog state from the available thermal emissive bands, the network was trained with ground-based fog retrievals based on leaf-wetness sensor measurements and other meteorological data from weather stations deployed throughout the Atacama Desert (Hoffmeister, 2017; Schween et al., 2020). Both satellite platforms are in polar orbits passing over the study region two times almost every day. For the fog retrieval, nocturnal overpass times are considered, which range between 2230 and 0010 Chile standard time (CLT) (Terra) and 0110 and 0245 CLT (Aqua) depending on orbit characteristics. The data set is available at a 1 km horizontal resolution. Here, we extend the 3-year record created in Böhm et al. (2021) to a 19-year record (2003−2021) to derive a robust climatological mean fog frequency. The corresponding satellite pixels for the locations of *T. landbeckii* populations were identified via nearest-neighbour matching.

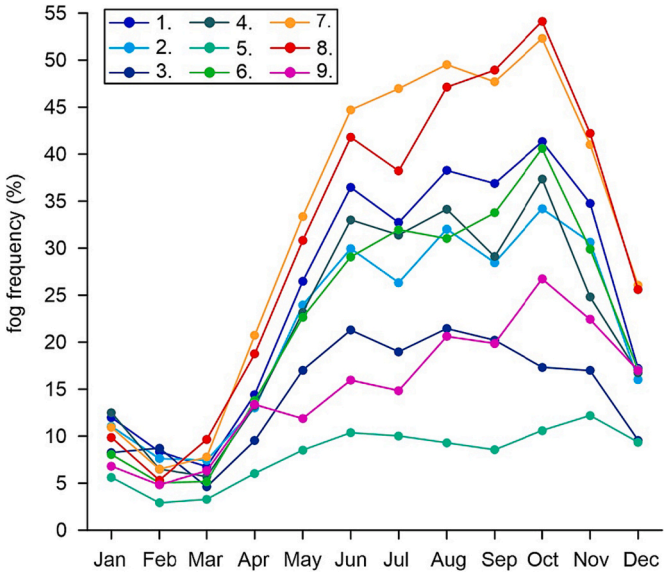

Fig. 2. Climatology of nocturnal fog frequency (19-year mean) based on satellite data and machine learning techniques according to Böhm et al. (2021). Shown are monthly fog frequencies at the nine different *T. landbeckii* sites (Fig. 1) according to Jaeschke et al. (2019).

2.3. Lipid biomarker analysis

Plant material was first rinsed with deionised water to remove surficial mineral dust and particles and then dried in a convection oven at 40 °C. Ground plant tissue (ca. 1 g) of in total 68 samples was ultrasonically extracted using a mixture of dichloromethane (DCM) and methanol (2:1, *v*/v), 3 times repeated. The extracts were combined and the bulk of the solvent removed by rotary evaporation under vacuum. The resulting total lipid extracts (TLE) were separated into apolar (with *n*-hexane), and polar (with DCM:methanol; 1:1, v/v) fractions using activated silica gel chromatography. The apolar fractions containing *n*-alkanes were further separated into saturated and unsaturated compounds using small columns filled with $AgNO_3$ coated silica gel (10% *w*/w) and *n*-hexane and DCM, respectively.

n-Alkanes were analyzed using a gas chromatograph equipped with an on-column injector and a flame ionization detector according to the method described in Contreras et al. (2022). A fused silica capillary column (DB-5MS; 50 m × 0.2 mm, film thickness: 0.33 μm) was used with He as carrier gas. Samples were injected at 70 °C and the GC oven temperature was subsequently raised to 150 °C at a rate of 20 °C/min, and then at 6 °C/min to 320 °C (held 40 min). Identification of *n*-alkanes was based on retention time in comparison with those of an alkane (*n*-C_{21}- *n*-C_{40}) standard solution. Analytical precision of the *n*-alkane quantifications based on replicate standard analyses was < 5%.

2.4. n-Alkane δD and $\delta^{13}C$ analysis

Compound-specific carbon ($\delta^{13}C$) and hydrogen (δD) isotope analyses of the most abundant *n*-alkane homologues (*n*-C_{23} - *n*-C_{31}) were performed on a Thermo Trace GC coupled to a Thermofisher MAT 252 ($\delta^{13}C$) and a MAT 253 (δD) isotope ratio mass spectrometer (IRMS) via a GC/C III combustion interface operated at 1000 °C ($\delta^{13}C$) and a GC IsoLink with a pyrolysis reactor operated at 1420 °C (δD), respectively. The GCs were equipped with 30 m × 0.25 mm columns (Restek Rxi-5 ms, film thickness: 1.0 μm) and He was used as the carrier gas. The methods used in this study followed those described in Jaeschke et al. (2020). Each sample was analyzed in duplicate if sufficient material was available. Isotope values were calibrated against reference gas using H_2 for δD and CO_2 for $\delta^{13}C$ and are reported in ‰ relative to Vienna Standard Mean Ocean Water (VSMOW) and Vienna Peedee Belemnite (VPDB), respectively. The long-term precision monitored by external standard analyses was < 0.3‰ for $\delta^{13}C$ and < 3‰ for δD.

2.5. Cellulose extraction and isotopic analysis

Dried plant material was ground in a ball mill (MM2, Retsch) to guarantee homogeneity of the sample for subsampling. Cellulose was chemically extracted from subsamples (n = 87) using the cuprammonium solution (CUAM) protocol as described in Wissel et al. (2008). The CUAM protocol comprises a wet oxidation step of the sample material with sodium chlorite ($NaClO_2$, pH 3, for 10 h at 60 °C) followed by a purification step for the residue via dissolution in cuprammonium

solution ($[Cu(NH_3)_4](OH)_2{\cdot}3H_2O$) and subsequent precipitation of dissolved cellulose with sulphuric acid (H_2SO_4, 20%). This protocol ensures that the extracted cellulose is free of any organic and inorganic contamination which otherwise would distort the genuine cellulose oxygen isotope value.

A varying amount of the extracted cellulose (<10 mg) was treated with 3 ml nitrating acid (65% fuming nitric acid, 35% phosphoric acid with phosphorus pentoxide (103–105%) to remove easily exchangeable hydroxyl-bound hydrogen (Alexander and Mitchell, 1949). The mixture was kept cool (5–7 °C) for 16 h and then filled up to 50 ml with deionised water of the same temperature to stop nitration. After centrifugation and decantation, the nitrated cellulose (NC) was washed 2–3 times with deionised water at room temperature to completely remove the reagent. The NC was then freeze dried and kept dry until measurement. According to the C/N ratio of NC the degree of nitration was 94 ± 2%.

For $\delta^{13}C$ analyses about 250 μg of bulk plant organic matter (OM) or cellulose was weighed in tin foil capsules. Samples were combusted at 1050 °C with excess oxygen in an elemental analyser (EuroEA, Eurovector, Italy) and measured online with a coupled isotope ratio mass spectrometer (IsoPrime, GV-Instruments, UK). Carbon content was determined by peak integration (*m/z* 44 and 45) and calibrated against a certified elemental standard. The International Atomic Energy Agency (IAEA) reference standards IAEA-CH6 ($\delta^{13}C = -10.45‰$) and IAEA-CH7 ($\delta^{13}C = -32.15‰$), and the United States Geological Survey (USGS) standard USGS24 ($\delta^{13}C = -16.05‰$) were used for calibrating laboratory isotope standards and to scale-normalize raw data.

For $\delta^{18}O$ analyses about 275 μg of cellulose was weighed in silver capsules, crimped and stored for at least 24 h in a vacuum drier at 110 °C before analyses. Samples were pyrolysed at 1450 °C in a high-temperature pyrolysis analyser (HT-O, HEKAtech, Germany) and measured on-line with a coupled isotope-ratio mass spectrometer (Isoprime, GV Instruments). Oxygen content was determined by peak integration (*m/z* 28 and 29) and calibrated against a certified elemental standard. The reference standards IAEA-601 ($\delta^{18}O = 23.14‰$) and IAEA-602 ($\delta^{18}O = 71.28‰$) were used for calibrating laboratory isotope standards and to scale-normalize raw data. Laboratory standards were IAEA-CH6 cellulose ($\delta^{18}O = 37.09 \pm 0.09‰$), cellulose from Merck ($\delta^{18}O = 27.97 \pm 0.08‰$), chitin from Sigma Aldrich ($\delta^{18}O = 24.11 \pm 0.16‰$) and lake cellulose ($\delta^{18}O = 17.74 \pm 0.28‰$).

For δD analyses about 600 μg of CN (equivalent to *c*. 14–15 μg hydrogen) and 1–2 mg of fine-grained (< 200 μm) chrome were weighed in silver capsules, crimped and stored for at least 12 h in a vacuum drier at 110 °C before analyses (Gehre et al., 2015). Samples were pyrolysed at 1450 °C in a high temperature pyrolysis analyser (HT-O, HEKAtech) and measured on-line with a coupled isotope ratio mass spectrometer (Isoprime, GV Instruments). Hydrogen content was determined by peak integration (*m/z* 1 and 2) and calibrated against a certified elemental standard. The reference standards USGS67 ($\delta D = -174.6‰$) and USGS68 ($\delta D = -10.2‰$) as well as IAEA-CH7 ($\delta D = -100.3‰$) were used for calibrating laboratory standards and to scale-normalize raw data. Laboratory standards were polyethylene foils PE-LD1 ($\delta D = -93.7 \pm 1.0‰$), PE-LD2 ($\delta D = -52.8 \pm 1.0‰$), and PE-LD4 ($\delta D = -113.6 \pm 1.0‰$), ground polyethylene ($\delta D = -70.2 \pm 1.0‰$).

Isotope data are reported in δ-notation (‰):

$$\delta = (R_S/R_{St}{-}1) \times 1000$$

with R_S as the isotope ratio ($^{13}C/^{12}C$ or $^{18}O/^{16}O$) of the sample and R_{St} as the isotope ratio of the respective standard. The overall precision of replicate analyses ($n > 6$) was < 0.1‰ for $\delta^{13}C$, < 0.25‰ for $\delta^{18}O$, and < 2.0‰ for δD derived from the above-mentioned standards.

2.6. Apparent fractionation

The apparent or net fractionation ($\varepsilon_{c/w}$) between measured isotope values in the plant organic compounds and supplied water was defined as enrichment:

$$\varepsilon_{c/w} = \alpha_{c-w} - 1 = (\delta_c + 1)/(\delta_w + 1) - 1$$

where α is the isotopic fractionation factor, δ_c is the isotopic composition of the respective compound (i.e., cellulose/*n*-alkanes) and δ_w is the isotopic composition of the water source ($\delta^{18}O_p$, δD_p). $\varepsilon_{c/w}$ represents the sum of multiple fractionation processes, such as leaf water enrichment through transpiration and biosynthesis of leaf organic compounds (Sternberg, 2009; Sachse et al., 2012).

2.7. Environmental reference data

The Online Isotopes in Precipitation Calculator (OIPC) was used to estimate the modern mean annual oxygen and hydrogen isotopic composition of precipitation ($\delta^{18}O_p$ and δD_p, respectively) based on the site location (i.e., latitude, longitude) and elevation (Supplementary Fig. 2) (Bowen and Revenaugh, 2003; Bowen, 2022). In general, $\delta^{18}O_p$ and δD_p reflect the fractionation of the respective isotopes during atmospheric vaporization and condensation processes on circulation pathways (Bowen and Revenaugh, 2003). The long-term average geospatial distribution of both, $\delta^{18}O_p$ and δD_p should thus reflect the average climatology of a region. Globally, rain and fog show distinct isotopic compositions, which reflect the different atmospheric transport histories of moisture. However, the difference between fog and rain can be less pronounced in some coastal areas or in orographic clouds, where both plot parallel to the global meteoric water line (GMWL) (Supplementary Fig. 3; Scholl et al., 2011). Since no long-term measurements are available for our specific sites, we rely on interpolated precipitation isotope values, which are associated with a relatively large error (Supplementary Fig. 2). Although limited temporal and spatial observations can result in inaccurate assessment of modelled precipitation isotope values (Araguás-Araguás et al., 2000), they are generally in good agreement with measured isotope values of meteoric water (Bowen and Revenaugh, 2003; Sachse et al., 2012; Ladd et al., 2021; Gaviria-Lugo et al., 2023).

3. Results

3.1. Patterns of fog occurrence over the past 19 years

The annual cycle of nocturnal fog occurrence at the nine *T. landbeckii* sites is shown in Fig. 2 as the long-term mean (2003–2021). It revealed a distinct seasonal cycle with generally high fog frequencies between May and November (12 to 54% average) and fog minima during austral summer (January–February-March ca. 6% average) considering all *T. landbeckii* sites across the coastal transect. Fog events were most frequent at the lower elevation sites at the coastal cliff (sites 7, 8) and generally decreased further inland and with elevation (Table 1), in accordance with observations from Alto Patache and Cerro Oyarbide (Del Rio et al., 2021; García et al., 2021).

The vertical distribution of liquid water content (LWC) in the stratocumulus cloud measured at Iquique airport is shown in Supplementary Fig. 4. A maximum of water availability appeared at ~1000 m asl considering all observations. This is a very first indication of vertical moisture distribution as the cloud and its LWC will be modified when interfering as fog with the surface (see Supplementary information 4).

3.2. Carbon isotopic composition of leaf organic compounds

$\delta^{13}C$ values of bulk plant OM ($\delta^{13}C_{OM}$) varied from −11.7‰ to −14.1‰ (Supplementary Table 1). Site-averaged $\delta^{13}C_{OM}$ values ranged between −12.4‰ and − 13.5‰ (Table 2). Similarly, $\delta^{13}C$ values of cellulose ($\delta^{13}C_{cell}$) revealed little variation between −10.0‰ and − 12.4‰ (Supplementary Table 1). At the site level, $\delta^{13}C_{cell}$ ranged between −10.8‰ and − 11.9‰ (Table 2). Compound-specific $\delta^{13}C$ values

Table 1
Location and environmental data of *Tillandsia landbeckii* sites across the coastal Atacama Desert. Temperature (T), precipitation (P) and actual surface evaporation (E) derived from a regional long-term weather simulation (Reyers et al., 2021) using the Weather Research and Forecasting Model (WRF; Skamarock et al., 2008) are given as climatological annual means over 20 years (Jaeschke et al., 2019; Contreras et al., 2022). A 19-year record of annual fog occurrence estimates is based on satellite data.

Site	Latitude (°S)	Longitude (°W)	Elevation (m asl)	Distance (km)	T (°C)	P (mm/y)	E (mm/y)	P/E	Fog (%)
1	18°28′37.6”	70°04′51.5”	1000	23.6	13.7	1.5	5.6	0.3	26
2	18°52′31.4”	70°07′12.9”	1043	21.7	16.3	1.1	5.7	0.2	22
3	19°04′21.9”	70°06′26.8”	1100	20.8	16.0	1.1	5.3	0.2	15
4	20°20′08.8”	70°01′54.3”	1065	12.7	15.4	1.0	3.6	0.3	22
5	20°31′30.6”	70°02′43.0”	1150	16.2	15.1	0.7	3.5	0.2	8
6	20°43′33.7”	69°58′13.8”	1016	24.0	15.0	0.5	3.3	0.1	22
7	21°10′40.6”	70°00′31.3”	930	10.1	14.4	0.6	4.9	0.1	32
8	21°18′22.7”	70°01′32.8”	990	3.2	13.8	0.5	4.8	0.1	31
9	21°24′38.5”	69°48′33.2”	1028	27.4	14.7	0.6	3.4	0.2	15

Table 2
Site-averaged isotopic composition of meteoric water ($\delta^{18}O_p$, δD_p) obtained with OIPC (Bowen, 2022), stable isotope compositions of leaf cellulose and leaf wax *n*-alkanes in *Tillandsia landbeckii*. The apparent fractionation between plant organic compounds and the source water ($\varepsilon_{c/w}$) were calculated for cellulose ($\delta^{18}O_{cell}$, δD_{cell}) and *n*-alkanes (δD_{wax}). Estimates of leaf water ^{18}O-enrichment are given as ε_{bio} - $\delta^{18}O$. Error indicate ±1SD.

Site	$\delta^{18}O_p$ (‰)	δD_p (‰)	$\delta^{18}O_{cell}$ (‰)	δD_{cell} (‰)	δD_{wax} (‰)	$\delta^{18}O_{cell}$ $\varepsilon_{c/w}$ (‰)	ε_{bio} - $\delta^{18}O$ (‰)	δD_{cell} $\varepsilon_{c/w}$ (‰)	δD_{wax} $\varepsilon_{c/w}$ (‰)	$\delta^{13}C_{cell}$ (‰)	$\delta^{13}C_{wax}$ (‰)	$\delta^{13}C_{OM}$ (‰)
1	−8.7 ± 1.2	−62 ± 11	29.7 ± 0.4	68 ± 4	−164 ± 2	38.8	8.3	138.9	−108.2	−11.6 ± 0.1	−22.3 ± 0.2	−12.7 ± 0.1
2	−8.5 ± 1.1	−60 ± 10	30.0 ± 0.4	50 ± 4	−166 ± 4	38.8	8.3	117.5	−112.9	−11.8 ± 0.3	−23.4 ± 0.5	−13.3 ± 0.3
3	−8.4 ± 1.0	−59 ± 10	30.0 ± 0.5	43 ± 3	−163 ± 4	38.6	8.2	108.7	−109.8	−11.9 ± 0.2	−23.3 ± 0.5	−13.1 ± 0.2
4	−5.7 ± 1.4	−40 ± 10	29.3 ± 0.5	40 ± 5	−168 ± 4	35.1	4.6	83.4	−133.9	−11.8 ± 0.2	−22.9 ± 0.4	−13.2 ± 0.2
5	−5.5 ± 1.4	−39 ± 10	29.9 ± 0.7	43 ± 8	−171 ± 6	35.6	5.1	85.4	−137.7	−11.8 ± 0.3	−23.3 ± 0.8	−13.5 ± 0.4
6	−4.9 ± 1.4	−34 ± 11	29.4 ± 0.5	41 ± 8	−165 ± 5	34.4	3.9	78.2	−135.2	−11.2 ± 0.4	−22.8 ± 0.5	−12.9 ± 0.4
7	−4.3 ± 1.4	−30 ± 11	29.2 ± 0.9	49 ± 12	−151 ± 3	33.6	3.1	81.7	−124.2	−10.8 ± 0.6	−22.5 ± 0.9	−12.4 ± 0.5
8	−4.4 ± 1.4	−30 ± 11	29.5 ± 0.4	37 ± 6	−155 ± 6	34.0	3.5	69.7	−128.1	−11.9 ± 0.3	−22.9 ± 0.5	−13.2 ± 0.3
9	−4.4 ± 1.3	−30 ± 11	29.6 ± 0.3	44 ± 5	−161 ± 4	34.1	3.6	76.5	−135.2	−11.7 ± 0.5	−22.9 ± 0.9	−13.1 ± 0.3

The apparent fractionation between measured isotope values in the plant organic compounds (cellulose and leaf wax *n*-alkanes) and supplied water as enrichment factors ($\varepsilon_{c/w}$) was defined as: $\varepsilon_{c/w} = \alpha_{c\text{-}w} - 1 = (\delta_c + 1) / (\delta_w + 1) - 1$; where α is the isotopic fractionation factor, δ_c is the isotopic composition of the organic compound and δ_w is the isotopic composition of the water source ($\delta^{18}O_p$, δD_p).
ε_{bio} - $\delta^{18}O$ = leaf water evaporative ^{18}O-enrichment assuming a nearly constant biosynthetic fraction of +30.5‰ for cellulose in *Tillandsia* (Helliker, 2014).

of the most abundant leaf wax *n*-alkanes (C_{23}-C_{31}; Supplementary Fig. 5a) ranged from −19.7‰ to −26.8‰ (Supplementary Table 2). The C_{31} *n*-alkanes had the most negative $\delta^{13}C$ values and the C_{23} *n*-alkanes the most ^{13}C-enriched values, while C_{25}-C_{29} *n*-alkanes revealed only minor differences in $\delta^{13}C$ (Supplementary Fig. 5b). Calculated site-averaged $\delta^{13}C$ values of the C_{23}-C_{31} *n*-alkanes ($\delta^{13}C_{wax}$) showed a narrow range between −22.3‰ and − 23.4‰ (Table 2). $\delta^{13}C_{wax}$ was offset from $\delta^{13}C_{OM}$ by about −10‰ and even −12‰ from $\delta^{13}C_{cell}$ (Table 2), but revealed a similar low variability of ca. 1‰ between the sites. Site-averaged $\delta^{13}C$ values of all organic compounds showed a negative relation with altitude, while $\delta^{13}C_{wax}$ is also negatively correlated with temperature (Figs. 3 and 4).

3.3. Hydrogen isotopic composition of leaf wax n-alkanes

Compound-specific δD values of the most abundant *n*-alkanes (C_{23}-C_{31}) ranged from −131‰ to −183‰ (Fig. 5; Supplementary Table 3) in the complete dataset ($n = 68$). The long-chain homologues revealed in general more negative δD values compared to the mid-chain *n*-alkanes (Supplementary Fig. 5c). The relatively high δD variation within individual *n*-alkanes of about 38–44‰ cannot be explained by changes in vegetation type or photosynthetic pathway and is thus likely reflecting natural variability of the *T. landbeckii* populations. As *n*-alkanes were almost evenly distributed (Supplementary Fig. 5a) and all isotopologues showed high inter-correlations ($R^2 = 0.9$; $p < 0.01$), we calculated for each site the weighted mean of C_{23}-C_{31} *n*-alkanes (δD_{wax}) to mitigate the high intra-system variability seen in individual *n*-alkane δD values. δD values of most likely dehydrated specimens at sites 6 and 7 were enriched by about 6–16‰ (Supplementary Fig. 6). We did not exclude the δD values of dehydrated specimens as they also reflect the long-term overall hydrological condition of each population. Site-averaged δD_{wax} values varied between −150‰ and − 171‰ (Fig. 5b; Table 2), and showed strong negative correlations with altitude (Fig. 3; Fig. 5). δD_{wax} was influenced by temperature to a much lesser degree compared to $\delta^{13}C_{wax}$. Moreover, a positive correlation was indicated between δD_{wax} and fog occurrence (Fig. 3; Supplementary Table 4).

3.4. Oxygen and hydrogen isotopic composition of leaf cellulose

The oxygen isotope composition of leaf cellulose ($\delta^{18}O_{cell}$) was enriched in ^{18}O and ranged between +28.2‰ and + 31.1‰ (Fig. 6; Supplementary Table 1) in the complete dataset ($n = 87$). A total variability of 2.9‰ was observed in between sites but also within the same site (Table 2). Mean $\delta^{18}O_{cell}$ was +29.5‰ ± 0.6‰. Lowest $\delta^{18}O_{cell}$ values were observed close to the coast and increased with distance and elevation, although these trends were not significant (Fig. 3;

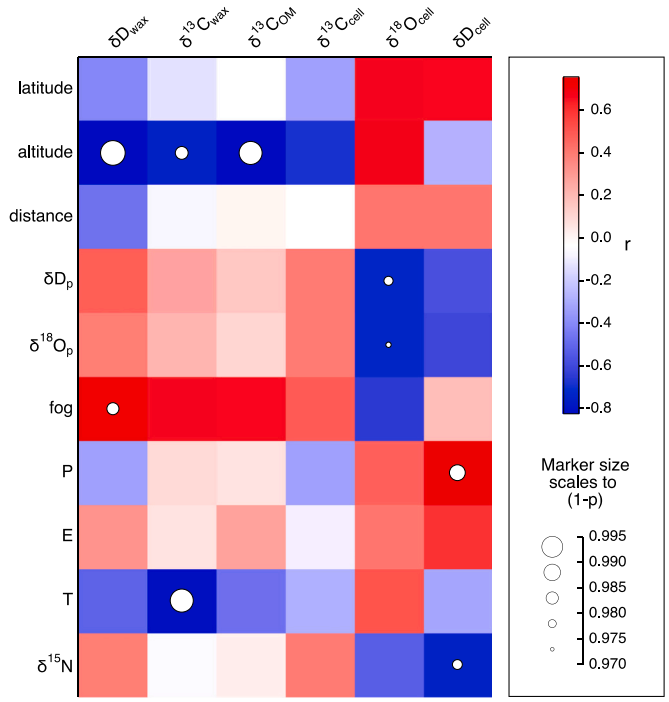

Fig. 3. Heat map showing Pearson correlation coefficients (r) and *p*-values for the different organic compounds in *T. landbeckii* and environmental variables as site averages. Note that *p*-values are given as 1-p, i.e., the size of the circle increases proportional to the significance. Precipitation (P), actual surface evaporation (E) and temperature (T) according to Table 1.

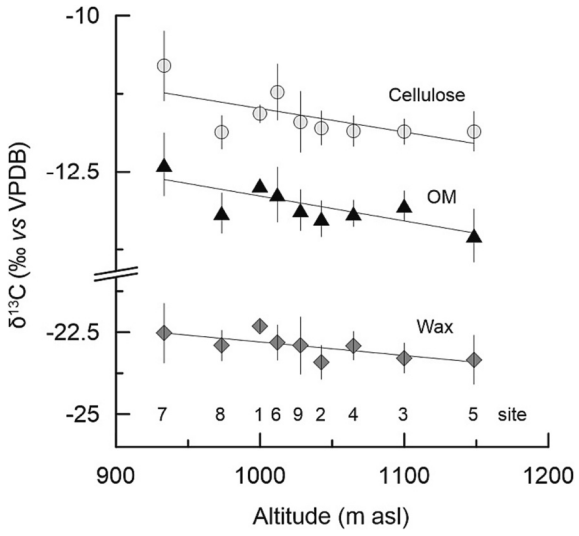

Fig. 4. Site-averaged $\delta^{13}C$ values of cellulose, bulk plant organic matter (OM), and leaf wax *n*-alkanes in *T. landbeckii* along elevation gradient. Error bars indicate ±1 SD. Numbers relate to the *T. landbeckii* sites (Fig. 1).

Supplementary Table 4). A low negative correlation was indicated between site-averaged $\delta^{18}O_{cell}$ and precipitation isotopes (Fig. 3; Supplementary Fig. 7).

The stable isotope composition of non-exchangeable hydrogen in cellulose (measured as cellulose nitrate, hereafter δD_{cell}) was strongly D-enriched with variations between +23‰ and + 74‰ (Fig. 6; Supplementary Table 1) in the complete dataset. Mean δD_{cell} values were + 43‰ ± 9‰. At the site level, the high isotopic enrichment in δD_{cell} compared to δD_{wax} resulted in large offsets of about 192–232‰ (Table 2). The net range in δD_{cell} of about 51‰ considering all individual measurements was similar to the variation in δD values of individual *n*-alkanes. Site-averaged δD_{cell} values were positively correlated with precipitation amount, and negatively correlated with foliar $\delta^{18}O$ values (Fig. 3; Supplementary Table 4).

There was only a weak correlation ($R^2 = 0.2$; $p < 0.01$) between $\delta^{18}O_{cell}$ and δD_{cell} (Fig. 6). Also, δD_{wax} showed no relation with either of the cellulose isotopes (Supplementary Table 4), which was also expressed in the different relationships between the isotopic markers and environmental variables (Fig. 3).

3.5. Apparent isotope fractionation along coastal transect

Apparent fractionation values ($\varepsilon_{c/w}$), shown as site-averages varied from −138‰ to −112‰ for δD_{wax} (Table 2). In cellulose, $\varepsilon_{c/w}$ values ranged from +33.6‰ to +38.8‰ for $\delta^{18}O_{cell}$, and from +70‰ to +139‰ for δD_{cell} (Table 2). Estimated leaf water ^{18}O-enrichment ranged from 3.1‰ to 8.3‰ at the site level (Table 2) assuming a nearly constant biosynthetic fractionation (ε_{bio}) of +30.5‰ for cellulose (Helliker, 2014). Highest evaporative enrichment was observed in all organic compounds at the northernmost sites 1–3, while all other sites exhibited a more similar range in $\varepsilon_{c/w}$, indicating less evaporative enrichment (Table 2; Fig. 6b). Similarly, $\varepsilon_{c/w}$ of all organic compounds revealed strong relationship with evaporation (Supplementary Fig. 8).

4. Discussion

4.1. Environmental influence on $\delta^{13}C$ values of leaf organic compounds

Strong CAM expression is reflected at all sites by highly ^{13}C-enriched values of bulk plant OM and cellulose in *T. landbeckii* (Table 2) compared to typical $\delta^{13}C$ values of C_3 plants or facultative CAM plants (Sternberg and De Niro, 1983; Hermida-Carrera et al., 2020). In contrast, $\delta^{13}C$ values of leaf wax *n*-alkanes are less distinctive from C_3 or C_4 plants in arid regions (Sternberg et al., 1984; Collister et al., 1994; Chikaraishi and Naraoka, 2003; Feakins and Sessions, 2010a) and may be a less suitable indicator of CAM activity. In general, $\delta^{13}C$ reflect the balance of photosynthesis and stomatal conductance and the coupled response to environmental conditions, i.e., water and nutrient availability, altitude, temperature (Warren et al., 2001; Diefendorf et al., 2010). Extremely low precipitation and strong evaporative gradients in the Atacama Desert require stomatal adaptation for regulating gas exchange, which shapes $\delta^{13}C$ values of both CAM and C_3 plants (Rundel et al., 1997; Ehleringer et al., 1998). In consequence, reduced stomatal conductance and low intercellular CO_2 values result in low rates of photosynthesis and subsequently slow growth rates of *T. landbeckii* as observed in the Oyarbide field (~13 mm/yr; Koch et al., 2020), which relates to our site 5.

All organic compounds reveal a similar systematic trend toward slightly more negative $\delta^{13}C$ values with increasing altitude (−0.4‰/100 m; Fig. 4) pointing to a physiological response to environmental conditions along the investigated gradient. Limitations in carbon assimilation can be related to lower temperatures (Diefendorf et al., 2010), which may also explain the changes in $\delta^{13}C$ within the investigated transect (Fig. 3). A study by Ehleringer et al. (1998) showed that $\delta^{13}C$ values of the coastal vegetation (mainly C_3 plants, some CAM plants) along an elevational transect near Paposo were most negative in the fog zone, consistent with higher humidity compared to the sites above/below the fog zone and thus indicating less drought stress for the plants. This elevational trend seen in our site-averaged $\delta^{13}C$ data may thus reflect the plants sensitive response to low vertical humidity gradients within the fog zone.

Other variables such as the slope of the terrain, stand density, nutrient status or plant lifecycle may as well affect carbon isotope discrimination (Warren et al., 2001). At steeper slopes, plants arranged in a typical banded pattern could tolerate lower moisture input and may more effectively capture fog moisture compared to sites with a more

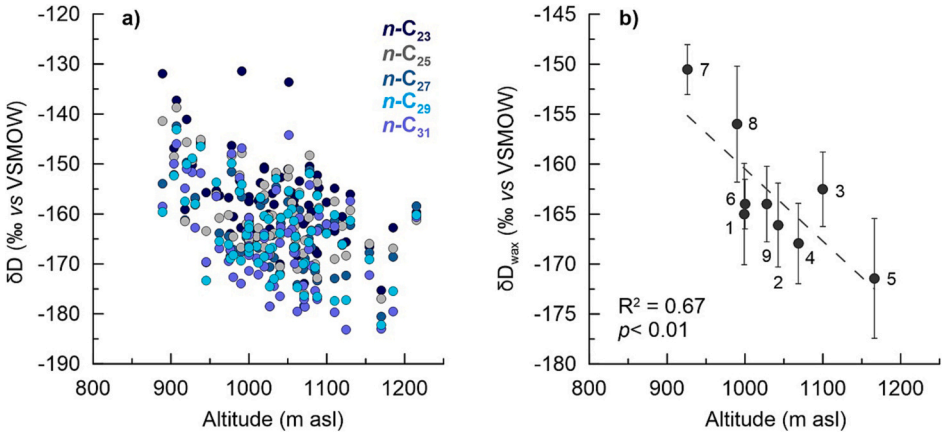

Fig. 5. a) δD values of individual leaf wax *n*-alkanes (all *T. landbeckii* sites) plotted against elevation; b) Site-averaged δD_{wax} values ±1 SD (weighted mean of C_{23}-C_{31} *n*-alkanes) indicate a significant negative correlation with elevation across a coastal transect between Arica and the Rio Loa canyon. Numbers relate to the *T. landbeckii* sites (Fig. 1).

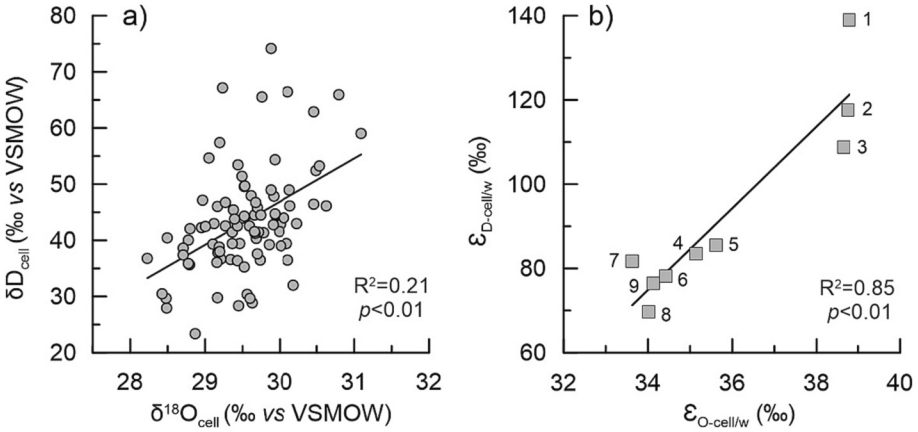

Fig. 6. a) Relationship of cellulose $\delta^{18}O$ values ($\delta^{18}O_{cell}$) and cellulose nitrate δD values (δD_{cell}) in *T. landbeckii* across the coastal Atacama Desert ($n = 87$); b) site-averaged oxygen and hydrogen isotope data presented as apparent fractionations ($\varepsilon_{c/w}$) between cellulose and source water. Numbers relate to the *T. landbeckii* sites (Fig. 1).

random distribution of isolated *T. landbeckii* stands or those growing on flat terrains (Borthagaray et al., 2010). *T. landbeckii* is adapted to a minimum average fog occurrence during the growing season and does not accept long-term stochasticity and extreme variations in fog events (Del Rio et al., 2021). This is probably best reflected at site 5, where nocturnal fog occurrence is extremely low compared to all other sites, but also most homogeneously distributed during the year (Fig. 2).

4.2. Biosynthetic, metabolic and physiological imprints on hydrogen and oxygen isotopes in leaf organic compounds

The different hydrological signals recorded in leaf wax *n*-alkanes and cellulose seem unexpected at first (Fig. 3). In general, source water and leaf water used for carbohydrate synthesis are impacted by climate. For instance, warm and dry conditions result in evaporative enrichment in both hydrogen and oxygen (Craig and Gordon, 1965; Farquhar et al., 2007; Kahmen et al., 2011; Cernusak et al., 2022). However, the source signal is not fully translated to cellulose or leaf waxes but is further modified by plant physiological and metabolic mechanisms (Yakir and DeNiro, 1990; Sternberg, 2009; Sachse et al., 2012; Cormier et al., 2018; Lehmann et al., 2021; Baan et al., 2023). Hence, we first need to explore biosynthetic pathways before we can interpret the different isotope ratios with respect to environmental parameters (Fig. 3).

Lipids are generally more D-depleted than cellulose, despite the fact that both organic precursor molecules originate from the same D-enriched triose-phosphate pools (Cormier et al., 2018). The offset relates to the different biosynthetic pathways and associated complex enzymatic reactions involving hydrogen transfer, which all can lead to strong isotopic fractionations (Hayes, 2001; Augusti et al., 2006; Sachse et al., 2012; Cormier et al., 2018). Consequently, large ranges of δD values between approximately −400‰ and + 200‰ can be observed in the resulting organic products (e.g., Sachse et al., 2012). Different proportions of hydrogen from multiple sources are going into biosynthesis of the organic compounds. For example, a higher proportion of D-depleted NADPH (nicotinamide adenine dinucleotide phosphate) produced in the chloroplast during the light reaction of photosynthesis is a critical source of hydrogen in lipid biosynthesis (~50%), while it accounts only for ~15% in carbohydrate biosynthesis (Cormier et al., 2018). In the acetogenic pathway for *n*-alkyl lipids, hydrogen in the initial butyryl chain originates from three sources: acetate (acetyl-CoA), NADPH and water. Sequential addition of acetyl-CoA units in the chloroplast then forms short chain fatty acids (typically n-C_{16} or n-C_{18}), followed by further elongation in the endoplasmic reticulum. There, decarboxylation of long-chain fatty acids to *n*-alkanes occurs, resulting in additional D-depletion in the order of −25‰ (Chikaraishi and Naraoka, 2007; Sachse et al., 2012). An important driver of the biosynthetic D-fractionation in cellulose may be related to the cycling of organic precursors pools (i.e., pyruvate and malic acid or hexose and triose) and the extraction of light hydrogen via the reduction of $NAD(P)^+$ (Cormier et al., 2018). Metabolic effects on post-photosynthetic D-fractionation in

the glycolysis-gluconeogenesis cycles can lead to more enriched δD values in cellulose compared to *n*-alkanes (Hayes, 2001; Luo and Sternberg, 1992; Sternberg et al., 1984; Cormier et al., 2018, 2019). Recent findings indicate that cellulose δD values are also strongly driven by D-fractionation in the photosynthesizing source cells. This was shown across plant species (Holloway-Phillips et al., 2022; Schuler et al., 2023) and within species (Baan et al., 2023; Wieloch et al., 2022a, 2022b). As such, the observed variation in *T. landbeckii* cellulose δD values may also reflect changes in the D-fractionation reactions occurring somewhere between CO_2 fixation and sucrose synthesis prior to its export to sink leaf tissue where cellulose is produced (Baan et al., 2023).

Significant differences between cellulose $\delta^{18}O$ and δD values (Fig. 6) could be expected as previous studies already indicated strong metabolic effects on D-fractionation in C_3 and CAM plants (Sternberg et al., 1984; Augusti et al., 2006; Cormier et al., 2018; Wieloch et al., 2022b; Baan et al., 2023). Some of the proposed biochemical mechanisms that cause isotopic enrichment during cellulose synthesis, namely exchange reactions with water during triose-hexose-phosphate cycling, occur for both oxygen and hydrogen (Yakir and DeNiro, 1990; Luo and Sternberg, 1992; Augusti et al., 2006; Cormier et al., 2018). However, the mechanisms for oxygen and carbon-bound hydrogen isotope exchange are different, such as hydrogen exchange with water always requires enzymes, whereas oxygen isotope exchange can occur via hydrogenation of the carbonyl group with water alone (Cormier et al., 2018; Holloway-Phillips et al., 2022). Also, isotopic fractionations between water and sugars before and during cellulose synthesis are more variable and less constant in δD compared to $\delta^{18}O$ (Yakir and DeNiro, 1990; Lehmann et al., 2021). Low photosynthetic carbohydrate supply may cause extreme isotopic enrichment seen in δD_{cell} (Table 2), resulting from higher exchange rates of carbon-bound hydrogen with D-enriched cellular water and the up-regulation of the oxidative pentose phosphate pathway (Yakir and DeNiro, 1990; Luo and Sternberg, 1992; Cormier et al., 2018, 2019). Thus δD_{cell} can provide important information on the carbon and energy metabolism of the plant (Sternberg and De Niro, 1983; Hayes, 2001; Cormier et al., 2018; Lehmann et al., 2021; Baan et al., 2023). Based on our results, we suggest that the low but significant correlation ($R^2 = 0.2$) between cellulose δD and $\delta^{18}O$ values (Fig. 6) may result from exchange with water for both oxygen and hydrogen (i.e., reflecting water $\delta^{18}O$ and δD values), altered by evaporative enrichment (Fig. 6b). The residual variation is most likely an effect of further D-fractionation through the many mechanisms that do not affect ^{18}O-fractionation.

4.3. Environmental influence on $\delta^{18}O_{cell}$ and δD_{wax}

The relatively narrow range in site-averaged $\delta^{18}O_{cell}$ values (Table 2) suggest fairly constant hydrological conditions over the entire coastal transect, i.e., minor changes in the Pacific Ocean source water. Due to the extremely low growth rates of the plants (Koch et al., 2020), $\delta^{18}O_{cell}$ may reflect a long-term integration of growing season $\delta^{18}O_p$ at the specific sites modified by evaporative enrichment (Kahmen et al., 2011; Helliker, 2014). As fog is believed to be the main moisture source, it should leave a prominent imprint on $\delta^{18}O_{cell}$ (Supplementary information 3). In conjunction with in general higher fog frequencies at the coastal cliff (García et al., 2021), site-averaged $\delta^{18}O_{cell}$ values can be explained by more frequent physical gas exchange in equilibrium with the Pacific source water, which may exceed net transpirational flux and dominate the isotopic signal on leaf water $\delta^{18}O$ (Lange and Medina, 1979; Helliker and Griffiths, 2007; Reyes-García et al., 2008; Mejia-Chang et al., 2021). Afternoon fog or moist maritime air may provide additional moisture for the plants (García et al., 2021), which is not captured by our current fog retrieval method.

In general, nocturnal net water vapor uptake during fog events should predominantly affect the isotopic signal (Mejia-Chang et al., 2021), although water uptake via trichomes can also occur during the day whenever humidity increase, despite stomatal closure. This can leave a strong ^{18}O-signal transfer into leaf water and assimilates as shown in a daytime fogging experiment with *T. usneoides* (Lehmann et al., 2019). Such strong ^{18}O-signal was suggested to relate to the low leaf water content or the uptake of liquid water by hydrophilic trichomes (Lehmann et al., 2019). The predicted $\delta^{18}O$ offset from tissue water can be as high as 2‰ at high humidity ('trichome offset'; Helliker, 2011). As the evaporative flux in CAM plants is generally low due to stomatal limitations, the water pool may become progressively enriched over time caused by less frequent gas exchange. This enrichment has been shown in mesocosm experiments with *T. fasciculata*, even in well-watered plants (Mejia-Chang et al., 2021). Our estimates of leaf water ^{18}O-enrichment of about 3–8‰ at the site level (using $\delta^{18}O_p$; Table 2) are comparable to those reported for different atmospheric CAM bromeliad species from Mexico, which indicated that water lost through transpiration over a five months drought led to an enrichment in leaf water $\delta^{18}O$ of only 3–6‰ compared to approximately 15‰ in C_3 plants (Reyes-García et al., 2008).

δD_{wax} in *T. landbeckii* is comparable to the few existing studies elaborating δD values in lipids of CAM plants, and similar to those of C_3 plants, which can be explained by the same biosynthetic pathway in the Calvin cycle (Sternberg et al., 1984; Chikaraishi and Naraoka, 2003; Feakins and Sessions, 2010b) but also to a lower metabolic sensitivity of D-fractionation during lipid biosynthesis compared to cellulose (Baan et al., 2023). Site-averaged δD_{wax} values show a strong negative correlation with elevation (Fig. 5b) and concur with trends seen in $\delta^{13}C$ values (Fig. 4). On the other hand, δD_{wax} shows no significant correlation with δD_p at the site level (Fig. 3). This lack of correlation is not surprising considering the extremely small range in precipitation (Table 1) and poorly constrained δD estimates of local precipitation in the study area (Table 2). This finding agrees with recent studies from the tropical Pacific and Chile south of our study area (Ladd et al., 2021; Gaviria-Lugo et al., 2023). In hyperarid regions, small variations in hydrological parameters can transform into large changes in δD compared to $\delta^{18}O$ (ratio 8:1; Craig, 1961). The proposed 'non-linearity' can then lead to overestimation of actual hydrological changes (Gaviria-Lugo et al., 2023). In addition, the availability of moisture for individual *T. landbeckii* specimen can be highly variable on small scales even within a site, introducing considerable scatter to δD_{wax}. Moreover, the contribution and isotopic composition of additional moisture sources such as fog, dew or atmospheric water vapor is not constrained at all and requires further investigation (see Supplementary information 3).

Following previous approaches (Ladd et al., 2021; Gaviria-Lugo et al., 2023), we examine *T. landbeckii* δD_{wax} values with respect to what is expected globally. To this end, we plotted δD values of the *n*-C_{29} alkane from both individual *T. landbeckii* specimens and as site averages together with the global dataset based on soils and sediments (Fig. 7) (Gaviria-Lugo et al., 2023). We added own unpublished *n*-C_{29} alkane δD data from individual *T. landbeckii* specimens collected from Peru and Chile south of the main study area (Supplementary Table 5) to extent our dataset outside the hyperarid core region. On a broader scale, δD_{wax} values generally follow the global linear relationship between δD_{wax} and δD_p and thus can be used as a predictor of δD_p. We note, however, that some of our δD_{wax} values plot above or below the global regression pointing to additional fractionation processes. This is also reflected in site-averaged δD_{wax} residuals (ΔD) calculated between measured and predicted δD_{wax} values of the *n*-C_{29} alkane from the global regression following the approach of Gaviria-Lugo et al. (2023). ΔD reveals a distinct pattern along the investigated gradient, with highest values of 4–8‰ at the northern sites 1–3 and lowest values between −7‰ and −19‰ at sites 4–9 (Fig. 7b), which equals changes seen in δD_{wax} with altitude (Fig. 5). Such relatively large deviations from the global regression suggest that the plants use a different additional moisture source such as fog or atmospheric water vapor, the latter a possible source of relatively D-depleted water (Araguás-Araguás et al., 2000; Feakins and Sessions, 2010b; Henze et al., 2022). Thus, different proportions of water vapor masses likely dominated by local fog-moisture

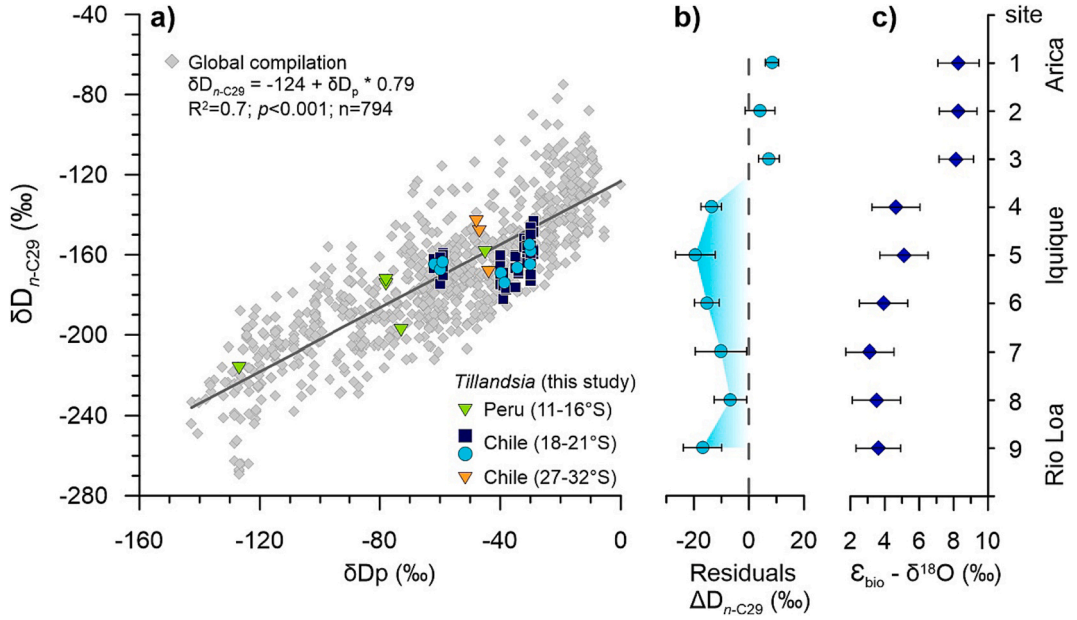

Fig. 7. a) δD values of *n*-C_{29} alkanes of individual *T. landbeckii* specimens from Chile and Peru (colored symbols, this study) plotted against δD_p. δD values of *n*-C_{29} alkanes are shown from individual specimens (dark blue squares) and as site averages (light blue circles). Grey diamonds represent *n*-C_{29} alkane δD values from a global compilation from soils and sediments (adapted and modified from Gaviria-Lugo et al., 2023). All mean annual δD_p estimates are derived from OIPC (Bowen and Revenaugh, 2003). b) calculated residuals (ΔD) from the nine *T. landbeckii* sites (*n*-C_{29} alkanes as site averages) with respect to the global regression. c) estimated leaf water ^{18}O enrichment (ε_{bio} - $\delta^{18}O$) from the nine *T. landbeckii* sites. Error bars indicate ±1 SD. (For interpretation of the references to colour in this figure legend, the reader is referred to the web version of this article.)

may impact the hydrological signal recorded in δD_{wax} across the investigated transect (Fig. 7b), which is in agreement with previous studies (Kahmen et al., 2011; Cernusak et al., 2022).

Typically, $\varepsilon_{c/w}$ is more negative in areas with higher relative humidity and lower evapotranspiration (Feakins and Sessions, 2010a; Polissar et al., 2009; Sachse et al., 2012). In our study area, the average $\varepsilon_{c/w}$ of −124‰ of *n*-alkanes in *T. landbeckii* is more negative than expected for arid to hyperarid regions, i.e., approximately −90‰ (Feakins and Sessions, 2010b; Gaviria-Lugo et al., 2023) but is well in the range of values reported globally (ca. -120‰; Sachse et al., 2012). Hyperaridity in our study area seems to cause less enrichment in *T. landbeckii* compared to C_3 plants, which is expected and can be explained by the unique water-saving strategies typical for CAM plants. The relationships of $\varepsilon_{c/w}$ and actual surface evaporation estimates further validates the effect of evaporative enrichment impacting the isotopic composition of all leaf organic compounds, mostly at the northern sites 1–3 (Table 2; Supplementary Fig. 8). Interestingly, δD_{wax} is correlated with both fog occurrence (Fig. 3) and estimated relative proportion of fog precipitation (P_{fog}; Supplementary Fig. 9). This further supports the notion that δD_{wax} reflects the balance of different vapor masses across the investigated gradients, which is not reflected in cellulose isotopes. Moreover, the influence of leaf water enrichment on $\delta^{18}O_{cell}$ (Fig. 7c) is not regarded a major factor that obscures the hydrological signal recorded in δD_{wax} (see also Kahmen et al., 2013).

4.4. Implications for hydroclimate reconstructions in the Atacama Desert

Past variations in fog/precipitation likely track large-scale changes in atmospheric circulation such as ENSO, which depends on latitude and altitude (e.g., Garreaud et al., 2008; Del Rio et al., 2021). As such, the response of the isotopic proxies is largely determined by the position of the *T. landbeckii* site within the humid fog zone and thus altitude (Fig. 3). A study by Del Rio et al. (2021) showed that during warm El Niño years, a higher inversion layer combined with the coastal topography may affect fog positively through lifting and cooling. This would be consistent with studies indicating increased fog water amounts at higher altitude (Cereceda et al., 2002; Garreaud et al., 2008; González et al., 2011; Zanetta et al., 2016; García et al., 2021). On decadal timescales covered by *T. landbeckii*, more summer fog and/or coastal rains may provide additional moisture at the high elevation sites 5–6 during the dry period (implying a different δD_p signal; Bowen and Revenaugh, 2003) and enhancing plant fitness (Koch et al., 2020). To this end, we compiled δD_{wax}, $\delta^{18}O_{cell}$, and δD_{cell} for distinct elevation intervals across the ca. 300 km coastal transect (Fig. 8). A slightly different picture emerges compared to the site-averaged distributions, where δD_{wax} and δD_p now show similar trends at the same elevation intervals. The isotope lapse rate of −3.7‰/100 m is similar in both δD_{wax} and δD_p within the main fog zone between 900 and 1200 m asl, indicating a high vertical gradient in δD observed for atmospheric water vapor (Araguás-Araguás et al., 2000). $\delta^{18}O_{cell}$ values are opposite in direction compared to $\delta^{18}O_p$ within the main fog zone (Fig. 8b) as already indicated before (Fig. 3; Supplementary Fig. 7), but changes in $\delta^{18}O_{cell}$ are much smaller (ca. +0.2‰/100 m). A possible explanation for the observed 'altitude effect' may relate to the gradual mixing of different water vapor masses along the transect (see previous section).

Surprisingly, foliar $\delta^{15}N$ data from the same set of samples (Jaeschke et al., 2019) reveal a similar trend as δD_{wax} and δD_p with most ^{15}N-depleted values at the highest elevation interval (Fig. 8c). $\delta^{15}N_{foliar}$ was proposed to decrease with increasing water and nitrogen nutrient sources (Latorre et al., 2011; Jaeschke et al., 2019), in accordance with the vertical moisture distribution in the cloud (Supplementary Fig. 3; Schween et al., 2022). However, we also note a large variability in $\delta^{15}N_{foliar}$ at the 1000–1100 m interval, and recent studies indicated the importance of microbial community composition associated with the plants/soils in shaping $\delta^{15}N_{foliar}$ (Alfaro et al., 2021; Jaeschke et al., 2023). δD_{cell} indicate more or less homogeneous values of ca. 42–43‰ in the main fog zone (Fig. 8d) pointing to relatively constant levels of photosynthetic carbohydrate supply (Cormier et al., 2019).

Most *T. landbeckii* specimens are derived from elevations between ca. 1000–1100 m in our study (Fig. 8), generally consistent with maximum LWC in the cloud (Supplementary Fig. 4). Considering seasonal changes in fog bank height and thickness (Schween et al., 2022), all sites at this

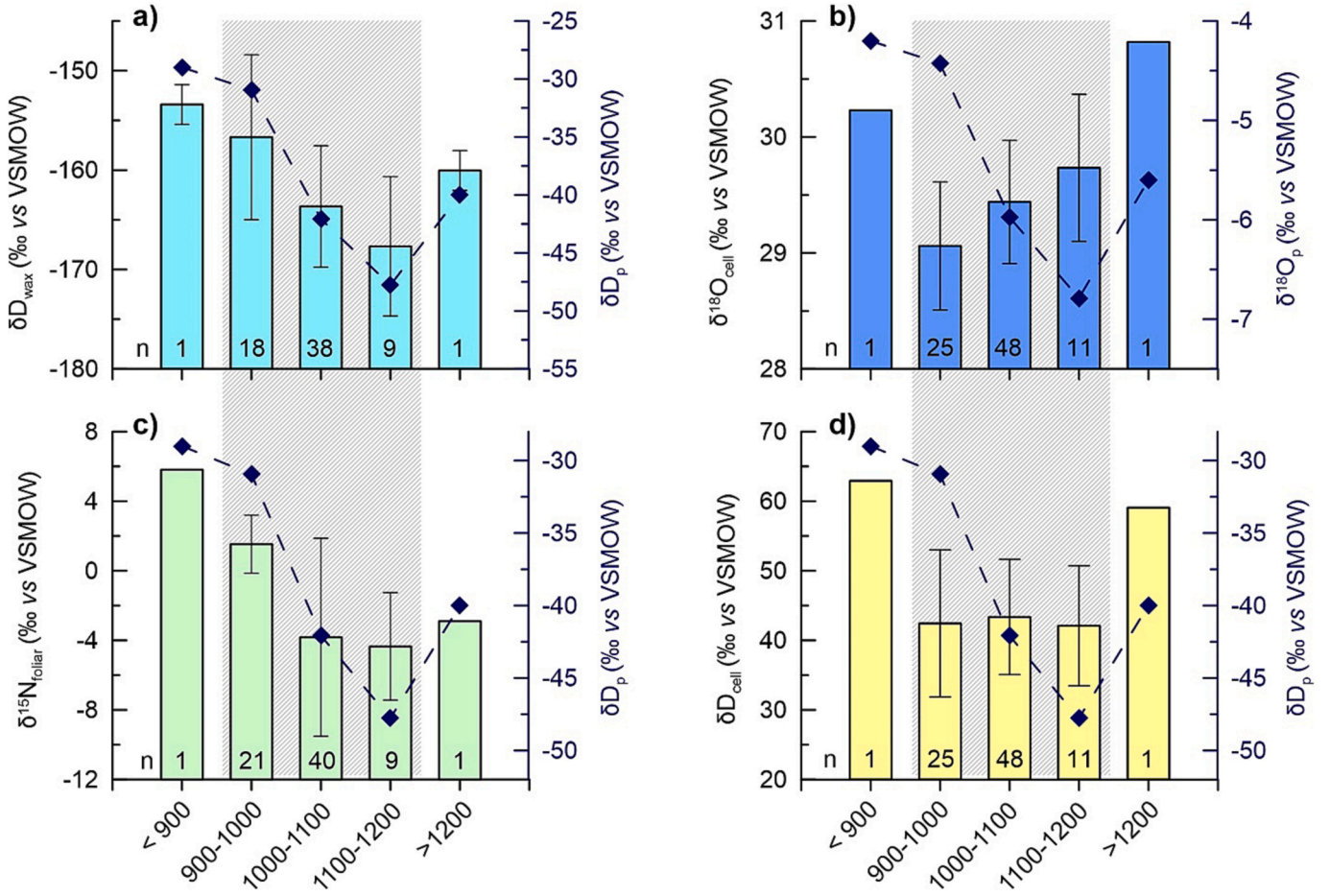

Fig. 8. Compilation of isotopic proxies for reconstructing hydrological changes across the coastal Atacama Desert between Arica and the Rio Loa canyon. Elevational trends in a) δD_{wax} b) $\delta^{18}O_{cell}$, c) foliar $\delta^{15}N$ (Jaeschke et al., 2019), and d) δD_{cell} are compared with meteoric water δD_p and $\delta^{18}O_p$ estimates (indicated as blue diamonds) obtained from OIPC (Bowen, 2022). Shown are average values ±SD for distinct elevation intervals (vertical bars), n refers to the number of *T. landbeckii* specimens analyzed. The extent of the main fog zone is indicated by grey shading. (For interpretation of the references to colour in this figure legend, the reader is referred to the web version of this article.)

elevation interval likely receive a well-balanced moisture amount during the year. Outside the main fog zone, other effects become more pronounced such as higher loss of water at the cloud top by evaporation of the dry, free troposphere (Schween et al., 2022). Sites currently located at the cloud base, would also receive less fog moisture on longer timescales. Higher aridity would then lead in both cases to the enrichment seen in all isotopic biomarkers (Fig. 8). Unfortunately, the upper/lower limits of the main fog zone are currently not sufficiently represented in our study. This needs further research as these plants may be particularly impacted by ongoing changes in fog frequencies (Del Rio et al., 2021).

5. Conclusion and outlook

We studied the stable carbon, hydrogen and oxygen isotopic composition of leaf organic compounds in fog-dependent *T. landbeckii* across the coastal Atacama Desert to determine correlations with environmental variables and to assess the applicability of the different proxies for hydroclimate studies in this extremely dry region. All organic compounds show ^{13}C-enriched isotopic signatures typical of CAM plants. The isotopic composition of leaf wax *n*-alkanes (δD_{wax}) and cellulose ($\delta^{18}O_{cell}$, δD_{cell}) seem modulated by both environmental and physiological/metabolic factors, thus complicating estimates of hydrologic conditions based on the systematic changes in $\delta^{18}O$ and δD of meteoric water. δD_{wax} reflects closest the hydrological balance in the study area and largely follows altitudinal changes in precipitation δD across the coastal Atacama Desert. Hence δD_{wax} can provide crucial information about past hydrological conditions at a specific site preserved in fossil *T. landbeckii* dune archives (see Jaeschke et al., 2023). In contrast, leaf water evaporative enrichment seems to have a dominant influence on $\delta^{18}O_{cell}$. Moreover, variation in δD_{cell} is beyond hydrological forcing but can provide important information on the carbon and energy metabolism of the plant. The plants that occur in a narrow elevational band of ca. 900–1200 m are potentially threatened by future climate change, i.e., precipitation anomalies, diminished cloud cover. Therefore, *T. landbeckii* sites presently located at the upper/lower limits of fog bank are prone to suffer dehydration and consequently dieback. This was indicated by the lowest elevation site 7, probably isolated from any fog moisture over a longer time period. All sites presently located within the main fog zone, however, seem to be well sustained by fog moisture. Investigations of more dune archives will allow to reconstruct past variations in hydrological conditions and to better constrain timescales of climate change impacting growth of *T. landbeckii* ecosystems. Future studies should include isotopic analyses of both leaf water and lipids/cellulose in living plants for the determination of biosynthetic and net fractionation values. Moreover, long-term assessment of fog water isotopic compositions is needed to better constrain variations in the source water across the coastal Atacama Desert. Finally, consideration of the full diurnal fog cycle, which is currently not available, would allow more genuine conclusions in the future.

CRediT authorship contribution statement

Andrea Jaeschke: Writing – review & editing, Writing – original draft, Investigation, Formal analysis, Conceptualization. **Christoph Böhm:** Writing – review & editing, Formal analysis, Conceptualization. **Jan H. Schween:** Writing – review & editing, Visualization, Formal analysis. **Enno Schefuß:** Writing – review & editing, Formal analysis. **Marcus A. Koch:** Writing – review & editing. **Claudio Latorre:** Writing – review & editing. **Sergio Contreras:** Writing – review & editing. **Janet Rethemeyer:** Funding acquisition. **Holger Wissel:** Formal analysis. **Andreas Lücke:** Writing – review & editing, Formal analysis, Conceptualization.

Declaration of competing interest

The authors declare that the research was conducted in the absence of any commercial or financial relationships that could be construed as a potential conflict of interest.

Data availability

All datasets generated in this study are included in the article and the Supplementary Files. Raw data will be made available in the CRC1211 database (www.crc1211db.uni-koeln.de).

Acknowledgements

We are grateful to Eduardo Campos and the colleagues at the Universidad Católica del Norte (UCN) in Antofagasta for logistic support. We thank Felix Merklinger for providing *Tillandsia* plant material from Peru, Ralph Kreutz for help with compound-specific isotope analyses and Christian Liebske for discussions. We also thank the two anonymous reviewers and the guest editor for constructive and helpful comments that significantly improved the quality of this manuscript. This study was part of the CRC 1211 'Earth – Evolution at the dry limit' supported by the German Research Foundation (DFG, grant number 268236062). CL acknowledges funding from ANID FB21006 to the IEB and ANID FONDECYT 1231820. Open Access funding enabled and organized by project DEAL.

Appendix A. Supplementary data

Supplementary data to this article can be found online at https://doi.org/10.1016/j.gloplacha.2024.104393.

References

Alexander, W.J., Mitchell, R.L., 1949. Rapid measurement of cellulose viscosity by the nitration method. Anal. Chem. 21, 1497–1500.

Alfaro, F.D., Manzano, M., Almiray, C., García, J.L., Osses, P., Del Rio, C., Vargas, C., Latorre, C., Koch, M.A., Siegmund, A., Abades, S., 2021. Soil bacterial community structure of fog-dependent *Tillandsia landbeckii* dunes in the Atacama Desert. Pl. Syst. Evol. 307, 56. https://doi.org/10.1007/s00606-021-01781-0.

Araguás-Araguás, L., Froehlich, K., Rozanski, K., 2000. Deuterium and oxygen-18 isotope composition of precipitation and atmospheric moisture. Hydrol. Process. 14, 1341–1355.

Aravena, R., Suzuki, O., Pollastri, A., 1989. Coastal fog and its relation to groundwater in the IV Region of northern Chile. Chem. Geol. 79, 83–91.

Arosio, T., Ziehmer-Wenz, M.M., Nicolussi, K., Schlüchter, C., Leuenberger, M., 2020. Larch Cellulose shows significantly Depleted Hydrogen Isotope Values with respect to Evergreen Conifers in Contrast to Oxygen and Carbon Isotopes. Front. Earth Sci. 8, 523073 https://doi.org/10.3389/feart.2020.523073.

Augusti, A., Betson, T.R., Schleucher, J., 2006. Hydrogen exchange during cellulose synthesis distinguishes climatic and biochemical isotope fractionations in tree rings. New Phytol. 172, 490–499.

Baan, J., Holloway-Phillips, M., Nelson, D.B., Kahmen, A., 2023. The metabolic sensitivity of hydrogen isotope fractionation differs between plant compounds. Phytochemistry 207, 113563. https://doi.org/10.1016/j.phytochem.2022.113563.

Benzing, D.H., Seeman, J., Renfrow, A., 1978. The foliar epidermis in Tillandsioideae (Bromeliaceae) and its role in habitat selection. Am. J. Bot. 65, 359–365. https://doi.org/10.2307/2442278.

Böhm, C., Schween, J.H., Reyers, M., Maier, B., Löhnert, U., Crewell, S., 2021. Toward a climatology of fog frequency in the Atacama Desert via multispectral satellite data and machine learning techniques. J. Appl. Meteorol. Climatol. 60, 1149–1169. https://doi.org/10.1175/JAMC-D-20- 0208.s1.

Borthagaray, A.I., Fuentes, M.A., Marquet, P.A., 2010. Vegetation pattern formation in fog-dependent ecosystem. J. Theoret. Biol. 265, 18–26.

Bowen, G.J., 2022. The Online Isotopes in Precipitation Calculator OIPC, version 2.2. Online available at: http://waterisotopes.org.

Bowen, G.J., Revenaugh, J., 2003. Interpolating the isotopic composition of modern meteoric precipitation. Water Resour. Res. 39, 1299.

Cereceda, P., Osses, P., Larrain, H., Farias, M., Lagos, M., Pinto, R., Schemenauer, R.S., 2002. Advective, orographic and radiation fog in the Tarapacá region, Chile. Atmos. Res. 64, 261–271.

Cereceda, P., Larraín, H., Osses, P., Farías, M., Egaña, I., 2008. The spatial and temporal variability of fog and its relation to fog oases in the Atacama Desert, Chile. Atmos. Res. 87, 312–323. https://doi.org/10.1016/j.atmosres.2007.11.012.

Cernusak, L.A., Barbeta, A., Bush, R.T., Eichstaedt, R., Ferrio, J.P., Flanagan, L.B., Gessler, A., Martin-Gomez, P., Hirl, R.T., Kahmen, A., Keitel, C., Lai, C.T., Munksgaard, N.C., Nelson, D.B., Ogée, J., Roden, J.S., Schnyder, H., Voelker, S.L., Wang, L., Stuart-Williams, H., Wingate, L., Yu, W., Zhao, L., Cuntz, M., 2022. Do ^{2}H and ^{18}O in leaf water reflect environmental drivers differently? New Phytol. 235, 41–51. https://doi.org/10.1111/nph.18113.

Chikaraishi, Y., Naraoka, H., 2003. Compound-specific dD–d^{13}C analyses of *n*-alkanes extracted from terrestrial and aquatic plants. Phytochemistry 63, 361–371.

Chikaraishi, Y., Naraoka, H., 2007. $\delta^{13}C$ and δD relationships among three n-alkyl compound classes (*n*-alkanoic acid, *n*-alkane and *n*-alkanol) of terrestrial higher plants. Org. Geochem. 38, 198–215.

Collister, J.W., Rieley, G., Stern, B., Eglinton, G., Fry, B., 1994. Compound-specific $\delta^{13}C$ analyses of leaf lipids from plants with differing carbon dioxide metabolisms. Org. Geochem. 21, 619–627.

Contreras, S., Landahur, M., García, K., Latorre, C., Reyers, M., Rethemeyer, J., Jaeschke, A., 2022. Leaf wax composition and distribution of *Tillandsia landbeckii* reflects moisture gradient across the hyper-arid Atacama Desert. Pl. Syst. Evol. 308, 8. https://doi.org/10.1007/s00606-021-01800-0.

Cormier, M.A., Werner, R.A., Sauer, P.E., Gröcke, D.R., Leuenberger, M.C., Wieloch, T., Schleucher, J., Kahmen, A., 2018. ^{2}H-fractionations during the biosynthesis of carbohydrates and lipids imprint a metabolic signal on the $\delta^{2}H$ values of plant organic compounds. New Phytol. 218, 479–491. https://doi.org/10.1111/nph.15016.

Cormier, M.A., Werner, R.A., Leuenberger, M.C., Kahmen, A., 2019. ^{2}H-enrichment of cellulose and n-alkanes in heterotrophic plants. Oecologia 189, 365–373. https://doi.org/10.1007/s00442-019-04338-8.

Craig, H., 1961. Isotopic variation in natural waters. Science 133, 1702–1703.

Craig, H., Gordon, L.I., 1965. Deuterium and oxygen-18 variations in the ocean and marine atmosphere. In: Tongiorgi, E. (Ed.), Stable Isotopes in Oceanographic Studies and Paleo-Temperatures. Laboratoria de Geologia Nucleare, Pisa.

Cushman, J.C., 2001. Crassulacean acid metabolism. A plastic photosynthetic adaptation to arid environments. Pl. Physiol. 127, 1439–1448.

Dansgaard, W., 1964. Stable isotopes in precipitation. Tellus 16, 436–468.

Del Río, C., Garcia, J.L., Osses, P., Zanetta, N., Lambert, F., Rivera, D., Siegmund, A., Wolf, N., Cereceda, P., Larraín, H., Lobos-Roco, F., 2018. ENSO influence on coastal fog-water yield in the Atacama Desert. Chile. Aerosol Air Qual. Res. 18, 127–144. https://doi.org/10.4209/aaqr.2017.01.0022.

Del Rio, C., Lobos-Roco, F., Latorre, C., Koch, M.A., Garcia, J.L., Osses, P., Lambert, F., Alfaro, F., Siegmund, A., 2021. Spatial distribution and interannual variability of coastal fog and low clouds cover in the hyperarid Atacama Desert and implications for past and present *Tillandsia landbeckii* ecosystems. Pl. Syst. Evol. 58, 1–23. https://doi.org/10.1007/s00606-021-01782-z.

Diefendorf, A.F., Freimuth, E.J., 2017. Extracting the most from terrestrial plant-derived n-alkyl lipids and their carbon isotopes from the sedimentary record: a review. Org. Geochem. 103, 1–21. https://doi.org/10.1016/j.orggeochem.2016.10.016.

Diefendorf, A.F., Mueller, K.E., Wing, S.L., Koch, P.L., Freeman, K.H., 2010. Global patterns in leaf ^{13}C discrimination and implications for studies of past and future climate. Proc. Natl. Acad. Sci. USA 107, 5738–5743.

Dodd, A.N., Borland, A.M., Haslam, R.P., Griffith, H., Maxwell, K., 2002. Crassulacean acid metabolism: plastic, fantastic. J. Exp. Bot. 53 (369), 569–580.

Eglinton, G., Hamilton, R.J., 1967. Leaf epicuticular waxes. Science 156, 1322.

Ehleringer, J.R., Rundel, P.W., Palma, B., Mooney, H.A., 1998. Carbon isotope ratios of Atacama Desert plants reflect hyperaridity of region in northern Chile. Rev. Chil. Hist. Nat. 71, 79–86.

Epstein, S., Thompson, P., Yapp, C.J., 1977. Oxygen and hydrogen isotopic ratios in plant cellulose. Science 198, 1209–1215.

Evans, S.E., Dueker, M.E., Logan, J.R., Weathers, K.C., 2019. The biology of fog: results from coastal Maine and Namib Desert reveal common drivers of fog microbial composition. Sci. Total Environ. 647, 1547–1556. https://doi.org/10.1016/j.scitotenv.2018.08.045.

Farquhar, G.D., Cernusak, L.A., Barnes, B., 2007. Heavy water fractionation during transpiration. Plant Physiol. 143, 11–18. https://doi.org/10.1104/pp.106.093278.

Feakins, S.J., Sessions, A.L., 2010a. Controls on the D/H ratios of plant leaf waxes from an arid ecosystem. Geochim. Cosmochim. Acta 74, 2128–2141.

Feakins, S.J., Sessions, A.L., 2010b. Crassulacean acid metabolism influences D/H ratio of leaf wax in succulent plants. Org. Geochem. 41, 1269–1276. https://doi.org/10.1016/j.orggeochem.2010.09.007.

García, J.L., Lobos-Roco, F., Schween, J.H., Del Rio, C., Osses, P., Vives, R., Pezoa, M., Siegmund, A., Latorre, C., Alfaro, F., Koch, M.A., Loehnert, U., 2021. Climate and coastal low-cloud dynamic in the hyperarid Atacama fog Desert and the geographic

distribution of Tillandsia landbeckii (Bromeliaceae) dune ecosystems. Pl. Syst. Evol. 307, 57. https://doi.org/10.1007/s00606-021-01775-y.
Garreaud, R., Barichivich, J., Christie, D.A., Maldonado, A., 2008. Interannual variability of the coastal fog at Fray Jorge relict forests in semi- arid Chile. J. Geophys. Res. 113, G04011. https://doi.org/10.1029/2008JG000709.
Gaviria-Lugo, N., Läuchli, C., Wittmann, H., Bernhard, A., Frings, P., Mohtadi, M., Rach, O., Sachse, D., 2023. Climatic controls on leaf wax hydrogen isotope ratios in terrestrial and marine sediments along a hyperarid to humid gradient. https://doi.org/10.5194/egusphere-2023-831.
Gehre, M., Renpenning, J., Gilevska, T., Qi, H., Coplen, T.B., Meijer, H.A.J., Brand, W.A., Schimmelmann, A., 2015. On-line hydrogen-isotope measurements of organic samples using elemental chromium: an extension for high temperature elemental-analyzer techniques. Anal. Chem. 87 (10), 5198–5205.
González, A.L., Fariña, J.M., Pinto, R., Pérez, C., Weathers, K.C., Armesto, J.J., Marquet, P.A., 2011. Bromeliad growth and stoichiometry: responses to atmospheric nutrient supply in fog-dependent eco- systems of the hyper-arid Atacama Desert, Chile. Oecologia 167, 835–845. https://doi.org/10.1007/s00442-011-2032-y.
Haslam, R., Borland, A., Maxwell, K., Griffiths, H., 2003. Physiological responses of the CAM epiphyte *Tillandsia usneoides* L. (Bromeliaceae) to variations in light and water supply. J. Pl. Physiol. 160, 627–634. https://doi.org/10.1078/0176-1617-00970.
Hayes, J., 2001. Fractionation of the isotopes of carbon and hydrogen in biosynthetic processes. In: Valley, J., Cole, D. (Eds.), National Meeting of the Geological Society of America. Boston, MA, pp. 225–271.
Helliker, B.R., 2011. On the controls of leaf-water oxygen isotope ratios in the Atmospheric Crassulacean Acid Metabolism Epiphyte *Tillandsia usneoides*. Pl. Physiol. 155, 2096–2107.
Helliker, B.R., 2014. Reconstructing the $\delta^{18}O$ of atmospheric water vapour via the CAM epiphyte *Tillandsia usneoides*: seasonal controls on $\delta^{18}O$ in the field and large-scale reconstruction of $\delta^{18}O_a$. Pl. Cell Environ. 37, 541–556.
Helliker, B.R., Griffiths, H., 2007. Toward a plant-based proxy for the isotope ratio of atmospheric water vapor. Glob. Chang. Biol. 13, 723–733.
Henze, D., Noone, D., Toohey, D., 2022. Aircraft measurements of water vapor heavy isotope ratios in the marine boundary layer and lower troposphere during ORACLES. Earth Syst. Sci. Data 14, 1811–1829. https://doi.org/10.5194/essd-14-1811-2022.
Hermida-Carrera, C., Fares, M.A., Font-Carrascosa, M., Kapralov, M.V., Koch, M.A., Mir, A., Molins, A., Ribas-Carbó, M., Rocha, J., Galmés, J., 2020. Exploring molecular evolution of Rubisco in C3 and CAM Orchidaceae and Bromeliaceae. BMC Evol. Biol. 20, 11. https://doi.org/10.1186/s12862-019-1551-8.
Hoffmeister, D., 2017. Meteorological and Soil Measurements of the Permanent Weather Stations in the Atacama Desert, Chile. Collaborative Research Centre CRC1211 Database. https://doi.org/10.5880/CRC1211DB.1 accessed 26 June 2020.
Holloway-Phillips, M., Baan, J., Nelson, D.B., Lehmann, M.M., Tcherkez, G., Kahmen, A., 2022. Species variation in the hydrogen isotope composition of leaf cellulose is mostly driven by isotopic variation in leaf sucrose. Plant Cell Environ. 45 (9), 2636–2651. https://doi.org/10.1111/pce.14362.
Houston, J., 2006. Variability of precipitation in the Atacama Desert: its causes and hydrological impact. Int. J. Climatol. 26, 2181–2198. https://doi.org/10.1002/joc.1359.
Houston, J., Hartley, A.J., 2003. The central Andean west-slope rain-shadow and its potential contribution to the origin of hyper-aridity in the Atacama Desert. Int. J. Climatol. 23, 1453–1464. https://doi.org/10.1002/joc.1359.
Jaeschke, A., Böhm, C., Merklinger, F.F., Bernasconi, S.M., Reyers, M., Kusch, S., Rethemeyer, J., 2019. Variation in $\delta^{15}N$ of fog-dependent *Tillandsia* ecosystems reflect water availability across climate gradients in the hyperarid Atacama Desert. Glob. Planet. Chang. 183, 103029 https://doi.org/10.1016/j.glop.lacha.2019.103029.
Jaeschke, A., Thienemann, M., Schefuß, E., Urban, J., Schäbitz, F., Wagner, B., Rethemeyer, J., 2020. Holocene hydroclimate variability and vegetation response in the ethiopian highlands (Lake Dendi). Front. Earth Sci. 8 (1–14), 2020. https://doi.org/10.3389/feart.2020.585770.
Jaeschke, A., May, S.M., Hakobyan, A., Mörchen, R., Bubenzer, O., Bernasconi, S.M., Schefuß, E., Hoffmeister, D., Latorre, C., Gwozdz, M., Rethemeyer, J., Knief, C., 2023. Microbial hotspots in a relict fog-dependent Tillandsia landbeckii dune from the coastal Atacama Desert. Glob. Planet. Chang. https://doi.org/10.1016/j.gloplacha.2024.104383.
Jetter, R., Kunst, L., Samuels, A.L., 2006. Composition of plant cuticular waxes. In: Riederer, M., Müller, C. (Eds.), Biology of the Plant Cuticle, Annual Plant Reviews 23. Blackwell Publishing, Oxford, pp. 145–181.
Jordan, T.E., Herrera, L.C., Godfrey, L.V., Colucci, S.J., Gamboa, P.C., Urrutia, M.J., González, L.G., Paul, J.F., 2019. Isotopic characteristics and paleoclimate implications of the extreme precipitation event of March 2015 in northern Chile. And. Geol. 46 (1), 1–31.
Kahmen, A., Sachse, D., Arndt, S.K., Tu, K.P., Farrington, H., Vitousek, P.M., Dawson, T. E., 2011. Cellulose $\delta^{18}O$ is an index of leaf-to-air vapor pressure difference (VPD) in tropical plants. Proc. Natl. Acad. Sci. USA 108, 1981–1986. https://doi.org/10.1073/pnas. 1018906108.
Kahmen, A., Hoffmann, B., Schefuß, E., Arndt, S.K., Cernusak, L.A., West, J.B., Sachse, D., 2013. Leaf water deuterium enrichment shapes leaf wax *n*-alkane δD values of angiosperm plants II: Observational evidence and global implications. Geochim. Cosmochim. Acta 111 (50), 63.
Koch, K., Ensikat, H.J., 2008. The hydrophobic coatings of plant surfaces: epicuticular wax crystals and their morphologies, crystallinity and molecular self-assembly. Micron 39, 759–772.
Koch, M.A., Kleinpeter, D., Auer, E., Siegmund, A., Del Rio, C., Osses, P., García, J.L., Marzol, M.V., Zizka, G., Kiefer, C., 2019. Living at the dry limits: ecological genetics of Tillandsia landbeckii Lomas in the Chilean Atacama Desert. Plant Syst. Evol. 305, 1041–1053. https://doi.org/10.1007/s00606-019-01623-0.
Koch, M.A., Stock, C., Kleinpeter, D., Del Río, C., Osses, P., Merklinger, F.F., Quandt, D., Siegmund, A., 2020. Vegetation growth and landscape genetics of Tillandsia Lomas at their dry limits in the Atacama Desert show fine-scale response to environmental parameters. Ecol. Evol. 10, 13260–13274. https://doi.org/10.1002/ece3.6924.
Kock, S.T., Schittek, K., Wissel, H., Vos, H., Ohlendorf, C., Schäbitz, F., Lupo, L.C., Kulemeyer, J.J., Lücke, A., 2019. Stable oxygen isotope records ($\delta^{18}O$) of a high-andean cushion Peatland in NW Argentina (24°S) imply South American Summer monsoon related moisture changes during the late holocene. Front. Earth Sci. 7, 45. https://doi.org/10.3389/feart.2019.00045.
Kurita, N., Ichiyanagi, K., Matsumoto, J., Yamanaka, M.D., Ohata, T., 2009. The relationship between the isotopic content of precipitation and the precipitation amount in tropical regions. J. Geochem. Explor. 102 (3), 113–122. https://doi.org/10.1016/j. gexplo.2009.03.002.
Ladd, S.N., Maloney, A.E., Nelson, D.B., Prebble, M., Camperio, G., Sear, D.A., Hassall, J. D., Langdon, P.G., Sachs, J.P., Dubois, N., 2021. Leaf wax hydrogen isotopes as a hydroclimate proxy in the tropical Pacific. J. Geophys. Res. Biogeosci. 126, e2020JG005891 https://doi.org/10.1029/2020JG005891.
Lange, O.L., Medina, E., 1979. Stomata of the CAM Plant *Tillandsia recurvata* Respond Directly to Humidity. Oecologia 40, 357–363.
Latorre, C., Gonzáles, A.L., Quade, J., Farina, J.M., Pinto, R., Marquet, P.A., 2011. Establishment and formation of fog-dependent Tillandsia landbeckii dunes in the Atacama Desert: evidence from radiocarbon and stable isotopes. J. Geophys. Res. 116, G03033. https://doi.org/10.1029/2010JG001521.
Lehmann, M.M., Goldsmith, G.R., Mirande-Ney, C., Weigt, R.B., Schönbeck, L., Kahmen, A., Gessler, A., Siegwolf, R.T.W., Saurer, M., 2019. The ^{18}O-signal transfer from water vapour to leaf water and assimilates varies among plant species and growth forms. Plant Cell Environ. 43, 510–523.
Lehmann, M.M., Vitali, V., Schuler, P., Leuenberger, M., Saurer, M., 2021. More than climate: Hydrogen isotope ratios in tree rings as novel plant physiological indicator for stress conditions. Dendrochronologia 65, 125788.
Lobos-Roco, F., Vilà-Guerau de Arellano, J., Pedruzo-Bagazgoitia, X., 2018. Characterizing the influence of the marine stratocumulus cloud on the land fog at the Atacama Desert. Atmos. Res. 214, 109–120.
Luo, Y.H., Sternberg, L., 1992. Deuterium heterogeneity in starch and cellulose nitrate of CAM and C3 plants. Phytochemistry 30, 1095–1098.
Lüttge, U., 2004. Ecophysiology of crassulacean acid metabolism (CAM). Ann. Bot. 93, 629–652.
Lüttge, U., 2010. Ability of crassulacean acid metabolism plants to overcome interacting stresses in tropical environments. AoB Plants 2010, plq005. https://doi.org/10.1093/aobpla/plq005.
Martin, C.E., 1994. Physiological ecology of the Bromeliaceae. Bot. Rev. 60, 1–82. https://doi.org/10.1007/BF02856593.
Mejia-Chang, M., Reyes-Garcia, C., Seibt, U., Royles, J., Meyer, M.T., Jones, G.D., Winter, K., Arnedo, M., Griffiths, H., 2021. Leaf water $\delta^{18}O$ reflects water vapour exchange and uptake by C_3 and CAM epiphytic bromeliads in Panama. Funct. Pl. Biol. 48, 732–742. https://doi.org/10.1071/FP21087.
MODIS Characterization Support Team, 2017a. MOD021KM-Level 1B Calibrated Radiances-1km. NASA MODIS Adaptive Processing System, Goddard Space Flight Center. https://doi.org/10.5067/MODIS/MOD021KM.061 accessed 31 December 2021.
MODIS Characterization Support Team, 2017b. MYD021KM-Level 1B Calibrated Radiances-1km. NASA MODIS Adaptive Processing System, Goddard Space Flight Center. https://doi.org/10.5067/MODIS/MYD021KM.061 accessed 31 December 2021.
Muñoz, R., Quintana, J., Falvey, M., Rutllant, J., Garreaud, R., 2016. Coastal clouds at the Eastern margin of the Southeast Pacific: Climatology and trends. J. Clim. 29, 4525–4542. https://doi.org/10.1175/JCLI-D-15-0757.1.
Pinto, R., Barria, I., Marquet, P.A., 2006. Geographical distribution of Tillandsia Lomas in the Atacama Desert, northern Chile. J. Arid Environ. 65, 543–552. https://doi.org/10.1016/j.jarid env.2005.08.015.
Polissar, P.J., Freeman, K.H., Rowley, D.B., McInerney, F.A., Currie, B.S., 2009. Paleoaltimetry of the Tibetan Plateau from D/H ratios of lipid biomarkers. Earth Planet. Sci. Lett. 287, 64–76.
Raux, P.S., Gravelle, S., Dumais, J., 2020. Design of a unidirectional water valve in *Tillandsia*. Nat. Commun. 11, 1–7. https://doi.org/10.1038/s41467-019-14236-5.
Reyers, M., 2019. WRF output daily Accumulated Precipitation 10 km Atacama. CRC1211 Database (CRC1211DB). https://doi.org/10.5880/CRC1211DB.20.
Reyers, M., Böhm, C., Knarr, L., Shao, Y., Crewell, S., 2021. Synoptic-to-Regional-Scale Analysis of Rainfall in the Atacama Desert (18°-26°S) using a Long-Term simulation with WRF. Mon. Weather Rev. 149, 91–149. https://doi.org/10.1175/MWR-D-20-0038.s1.
Reyes-García, C., Mejia-Chang, M., Jones, G.D., Griffiths, H., 2008. Water vapour isotopic exchange by epiphytic bromeliads in tropical dry forests reflects niche differentiation and climatic signals. Plant Cell Environ. 31 (6), 828–841.
Rundel, P.W., Dillon, M.O., 1998. Ecological patterns in the Bromeliaceae of the Lomas formations of Coastal Chile and Peru. Pl. Syst. Evol. 212, 261–278.
Rundel, P.W., Palma, B., Dillon, M.O., Sharifi, M.R., Nilsen, E.T., Boonpragob, K., 1997. *Tillandsia landbeckii* in the coastal Atacama Desert of northern Chile. Rev. Chil. Hist. Nat. 70, 341–349.
Sachse, D., Billault, I., Bowen, G.J., Chikaraishi, Y., Dawson, T.E., Feakins, S.E., Freeman, K.H., Magill, C.R., McInerney, F.A., Van der Meer, M.T.J., Polissar, P., Robins, R.J., Sachs, J.P., Schmidt, H.L., Sessions, A.L., White, J.W.C., West, J.B., Kahmen, A., 2012. Molecular paleohydrology: interpreting the hydrogen-isotopic

composition of lipid biomarkers from photosynthesizing organisms. Annu. Rev. Earth Planet. Sci. 40, 221–249.
Schefuß, E., Schouten, S., Schneider, R.R., 2005. Climatic controls on central African hydrology during the past 20,000 years. Nature 437 (7061), 1003–1006.
Schmitt, A.K., Martin, C.E., Lüttge, U.E., 1989. Gas exchange and water vapor uptake in the atmospheric CAM Bromeliad *Tillandsia recurvata* L.: the influence of trichomes. Bot. Acta 102, 80–84.
Scholl, M., Eugster, W., Burkard, R., 2011. Understanding the role of fog in forest hydrology: stable isotopes as tools for determining input and partitioning of cloud water in montane forests. Hydrol. Process. 25, 353–366.
Schuler, P., Vitali, V., Saurer, M., Gessler, A., Buchmann, N., Lehmann, M.M., 2023. Hydrogen isotope fractionation in carbohydrates of leaves and xylem tissues follows distinct phylogenetic patterns: a common garden experiment with 73 tree and shrub species. New Phytol. 239 (2), 547–561. https://doi.org/10.1111/nph.18976.
Schulz, N., Boisier, J.P., Aceituno, P., 2011. Climate change along the arid coast of northern Chile. J. Clim. 32, 1803–1814. https://doi.org/10.1002/joc.2395.
Schween, J.H., Hoffmeister, D., Loehnert, U., 2020. Filling the observational gap in the Atacama Desert with a new network of climate stations. Glob. Planet. Chang. 184, 103034 https://doi.org/10.1016/j.gloplacha.2019.103034.
Schween, J.H., Del Rio, C., Garcia, J.L., Osses, P., Westbrook, S., Löhnert, U., 2022. Life cycle of stratocumulus clouds over one year at the Coast of the Atacama Desert. Atmos. Chem. Phys. 22, 12241–12267. https://doi.org/10.5194/acp-2022-108.
Skamarock, W., Klemp, J., Dudhia, J., Gill, D., Barker, D., Wang, W., Huang, X.Y., Duda, M., Powers, G., 2008. A Description of the Advanced Research WRF Version 3. NCAR Tech., p. 113. https://doi.org/10.5065/d68s4mvh. Note NCAR/TN-475+STR.
Soderberg, K., 2010. The Role of Fog in the Ecohydrology and Biogeochemistry of the Namib Desert. PhD thesis. University of Virginia, USA.
Sternberg, L., 2009. Oxygen stable isotope ratios of tree-ring cellulose: the next phase of understanding. New Phytol. 181, 553–562.
Sternberg, L., De Niro, M.J., 1983. Isotopic composition of cellulose from C3, C4, and CAM plants growing near one another. Science 220, 947–949.
Sternberg, L., Deniro, M.J., Ajie, H., 1984. Stable hydrogen isotope ratios of saponifiable lipids and cellulose nitrate from CAM, C-3 and C-4 plants. Phytochemistry 23, 2475–2477.
Warren, C.R., McGrath, J.F., Adams, M.A., 2001. Water availability and carbon isotope discrimination in conifers. Oecologia 127, 476–481. https://doi.org/10.1007/s004420000609.
Westbeld, A., Klemm, O., Griessbaum, F., Strater, E., Larrain, H., Osses, P., Cereceda, P., 2009. Fog deposition to a Tillandsia carpet in the Atacama Desert. Ann. Geophys. 27, 3571–3576. https://doi.org/10.5194/angeo-27-3571-2009.
Wieloch, T., Augusti, A., Schleucher, J., 2022a. Anaplerotic flux into the Calvin-Benson cycle: hydrogen isotope evidence for in vivo occurrence in C3 metabolism. New Phytol. 234 (2), 405–411. https://doi.org/10.1111/nph.17957.
Wieloch, T., Grabner, M., Augusti, A., Serk, H., Ehlers, I., Yu, J., Schleucher, J., 2022b. Metabolism is a major driver of hydrogen isotope fractionation recorded in tree-ring glucose of *Pinus nigra*. New Phytol. 234 (2), 449–461. https://doi.org/10.1111/nph.18014.
Wissel, H., Mayr, C., Lücke, A., 2008. A new approach for the isolation of cellulose from aquatic plant tissue and freshwater sediments for stable isotope analysis. Org. Geochem. 39, 1545–1561. https://doi.org/10.1016/j.orggeochem.2008.07.014.
Yakir, D., DeNiro, M.J., 1990. Oxygen and Hydrogen Isotope fractionation during Cellulose Metabolism in *Lemna gibba* L. Plant Physiol. 93, 325–332.
Zanetta, N., Del Rio, C., Osses, P., Garcia, J.L., Luengo, Y., Wolf, N., Siegmund, A., 2016. Spatio-temporal variability of fog water and its meteorological conditions in the coastal Atacama Desert, Chile. In: Błaś, M., Sobik, M. (Eds.), 7th International Conference on Fog, Fog Collection and Dew. Wroclaw, Poland, 24–29 July, Proceedings Book. FFCD, Wroclaw, pp. 122–125.